International Journal of Robotics and Control Systems
Vol. 6, No. 1, 2026, pp. 423-453
ISSN 2775-2658
http://pubs2.ascee.org/index.php/ijrcs

Comparative Analysis of Intelligent PID Tuning Methods for Position Tracking in Mismatched Electro-Hydraulic Actuator

Thasvinthiran Balachandran [a,1], Siti Marhainis Othman [a,2,*], Muhamad Safwan bin Muhamad Azmi [b,3], Mohd Ariffanan Mohd Basri [c,4], Mohd Shuhanaz Zanar Azalan [c,5]

[a] Faculty of Electrical Engineering & Technology, Universiti Malaysia Perlis, 02600 Arau, Perlis, Malaysia
[b] Faculty of Mechanical Engineering & Technology, Universiti Malaysia Perlis, 02600 Arau, Perlis, Malaysia
[c] Faculty of Electrical Engineering, Universiti Technology Malaysia, 81310 Skudai, Johor, Malaysia
[1] thasvinthiran@studentmail.unimap.edu.my; [2] marhainis@unimap.edu.my; [3] safwanazmi@unimap.edu.my;
[4] shuhanaz@unimap.edu.my; [5] ariffanan@utm.my
* Corresponding Author

ARTICLE INFO

Article history
Received November 06, 2025
Revised January 12, 2026
Accepted February 06, 2026

Keywords
Sensor;
Controller;
Actuators;
Servo Position;
Control System;
Electro-Hydraulic;
Fuzzy;
MATLAB/Simulink

ABSTRACT

Electro-hydraulic actuators (EHAs) are widely applied in industrial motion control systems due to their high-power density and fast response. However, external disturbances make accuracy of the position control of EHAs challenging. Proportional–Integral–Derivative (PID) controllers are commonly used in practice, but their performance depends heavily on the tuning method. This study presents a comparative evaluation of four PID tuning techniques-Ziegler-Nichols (ZN), Particle Swarm Optimization (PSO), Adaptive Particle Swarm Optimization (APSO), and Fuzzy-PID (FPID) applied to a mismatched EHA system under mismatched operating conditions arising from external load disturbances, which enter the actuator dynamics through a mechanical state different from the control input channel rather than through the input voltage, thereby constituting a mismatched disturbance in the control-theoretic sense. All controllers are implemented in MATLAB/Simulink and tested using a step input reference under four external disturbance conditions. Performance is evaluated based on trajectory tracking accuracy, settling time, overshoot, steady-state error, and sum of squared error (SSE). Simulation results show that the conventional ZN-PID controller suffers from large overshoot, longer settling time, and higher SSE, particularly under increased disturbances. PSO-PID and APSO-PID improve transient response and reduce SSE; however, their performance degrades under severe disturbances. In contrast, the Fuzzy-PID controller consistently achieves the best overall performance. Compared with ZN-PID, the Fuzzy-PID reduces SSE by approximately 50–72% across all disturbance cases, while also yielding faster settling time, negligible overshoot, and minimal steady-state error. These results demonstrate that intelligent tuning approaches significantly enhance EHA position control performance. Among the evaluated methods, Fuzzy-PID provides the highest robustness and tracking accuracy under mismatched and disturbance-prone conditions, making it well suited for practical industrial EHA applications.

1. Introduction

Electro-hydraulic actuator (EHA) systems play a critical role in modern industrial, robotic, and automotive applications due to their compact design, high force output, and energy efficiency [1]. Typical applications include industrial manipulators, injection molding machines, flight simulators, automotive active suspension systems, and robotic motion platforms, where precise force and position control are required under varying load conditions. However, EHA performance is often hindered by strong nonlinearities, internal leakage, friction, valve dead zones, and parameter variations, which compromise stability, accuracy, and robustness [2]-[6].These challenges are further exacerbated under mismatched operating conditions, where discrepancies exist between the nominal model and the actual system dynamics. In practical EHAs, such mismatches may arise from unmodeled load friction, time-varying payload inertia, supply pressure fluctuations, valve leakage, or aging-induced parameter drift. Under such conditions, conventional fixed-gain controllers frequently fail to maintain consistent tracking performance, motivating the need for more robust control strategies [7]-[13].

In recent years, research interest in EHA control strategies has grown steadily, reflecting the increasing demand for high-performance and reliable actuation systems. As shown in Fig. 1, an analysis of Scopus data indicates that the number of publications related to EHA control systems increased from about 22,500 in 2019 to nearly 36,000 in 2024. This growth demonstrates the rising global importance of EHA research across multiple disciplines, including engineering, computer science, and applied mathematics. Leading contributions have been made by researchers such as Castillo O., Shi P., Blaabjerg F., Krstić M., and Guerrero J.M., with China, the United States, India, the United Kingdom, and Iran among the most active countries in this field. Such trends highlight the significance of EHA systems as a multidisciplinary research focus.

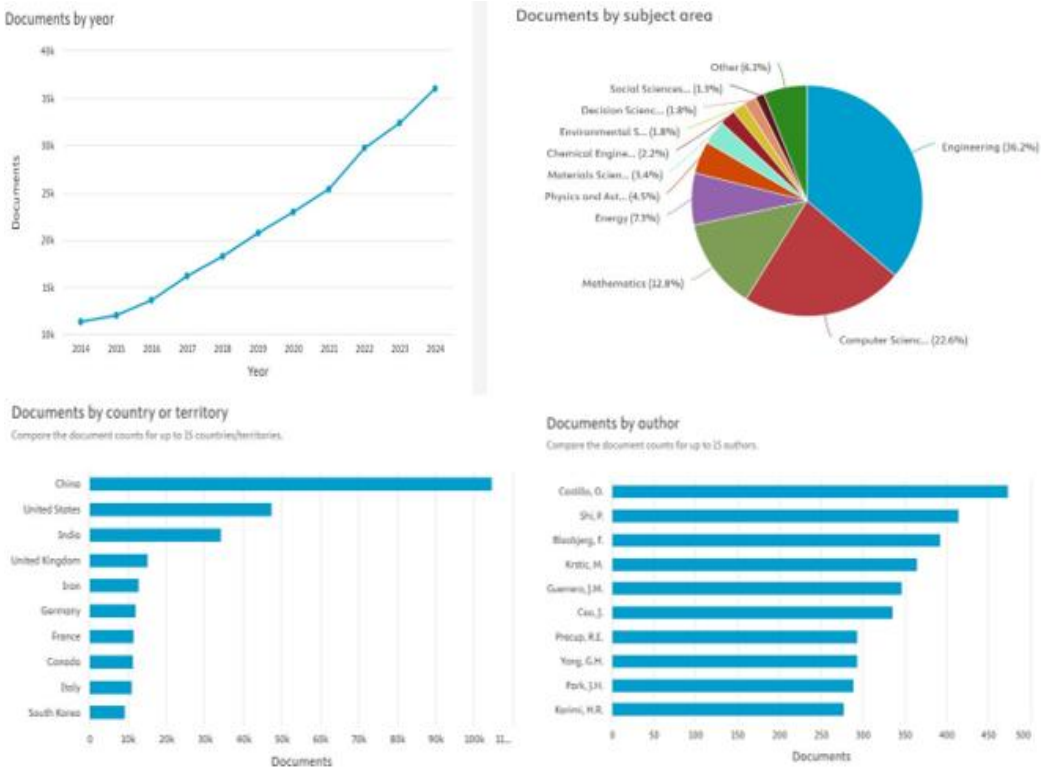

Fig. 1. Publication trends on control system in electro-hydraulic actuator system (2014-2024)

At the controller level, classical Proportional–Integral–Derivative (PID) controllers tuned using the Ziegler–Nichols (ZN) method remain widely adopted in industrial practice due to their simplicity and ease of implementation [14]-[18]. Nevertheless, ZN-tuned PID controllers are highly sensitive to nonlinearities, parameter variations, and external disturbances, resulting in excessive overshoot,

prolonged settling time, and degraded steady-state accuracy when operating conditions deviate from nominal assumptions. To address these limitations, metaheuristic-based optimization techniques such as Particle Swarm Optimization (PSO) and Adaptive Particle Swarm Optimization (APSO) have been increasingly explored for PID tuning [19]-[25]. PSO offers an effective global search capability with relatively low computational complexity, while APSO further enhances adaptability by dynamically adjusting swarm parameters to balance exploration and exploitation. These characteristics make APSO particularly suitable for control problems involving parameter uncertainty and time-varying dynamics, as encountered in mismatched EHA systems. In parallel, intelligent control approaches such as Fuzzy-PID controllers have demonstrated strong robustness against uncertainties and disturbances by incorporating heuristic rules and nonlinear gain adaptation mechanisms [26]-[30].

Although numerous studies have investigated ZN-PID, PSO-PID, APSO-PID, and Fuzzy-PID controllers individually for EHA applications, a systematic comparison of their performance under identical mismatched conditions and external disturbances remains limited. In particular, the relative robustness, adaptability, and tracking accuracy of APSO-PID in comparison with other tuning strategies under physically mismatched EHA scenarios have not been sufficiently evaluated using a unified framework.

The research contribution of this paper is to provide a comprehensive comparative assessment of four PID tuning approaches; ZN-PID, PSO-PID, APSO-PID, and Fuzzy-PID for position trajectory tracking of a mismatched EHA system subject to varying external disturbances. The comparison is conducted using a consistent MATLAB/Simulink simulation framework and evaluated based on trajectory tracking accuracy, transient performance metrics, and error-based indices. By identifying the tuning method that offers the best trade-off between robustness, adaptability, and control accuracy, this study aims to support the selection of reliable PID tuning strategies for practical industrial EHA applications. The remainder of the paper is organized as follows; Section 2 describes the system modeling and control methodology, Section 3 presents the simulation results and performance analysis, and Section 4 concludes the paper with key findings and future research directions.

2. Methodology

The phase of development of this project began with the mathematical modeling and derivation of the electro hydraulics system (EHA). Following that, the project moves on to the design phase, where the block diagram is designed using the parameters that were determined in the research phase. The EHA system is then modelled in the MATLAB Simulink based on the mathematical equation. The EHA system is a third-order nonlinear system that is substantially nonlinear because of system uncertainty. The fluid flow expression across the system, friction, and leakage coefficient are the three main system uncertainties that impair the system's performance. The PID controller is implemented to stabilize and optimize the EHA system. The controller's gains (K_P, K_I, K_D) were tuned using both the Ziegler-Nichols (ZN), Particle Swarm Optimization (PSO), Adaptive Particle Swarm Optimization (APSO) and the Fuzzy PID (FPID) methods. The performance of each tuning method was thoroughly assessed via MATLAB Simulink, with a focus on metrics like rise time, steady-state error, and overshoot. This comparative analysis aimed to determine the optimal tuning method for achieving superior tracking performance in the EHA system. The overall methodology of this study follows a structured workflow consisting of EHA system modeling, controller design and tuning using different approaches, application of external disturbance scenarios, and comparative performance evaluation using transient and error-based indices. A flowchart illustrating the complete methodological procedure is provided Fig. 2.

2.1. Mathematical Modelling of EHA System

The electro-hydraulic actuator (EHA) can be viewed as a hydraulic cylinder operated through a servo valve [31]-[37]. Functionally, it behaves like a piston connected to a load at its rod end, but

without additional springs or dampers. The servo valve regulates the piston movement, which in turn drives the external load.

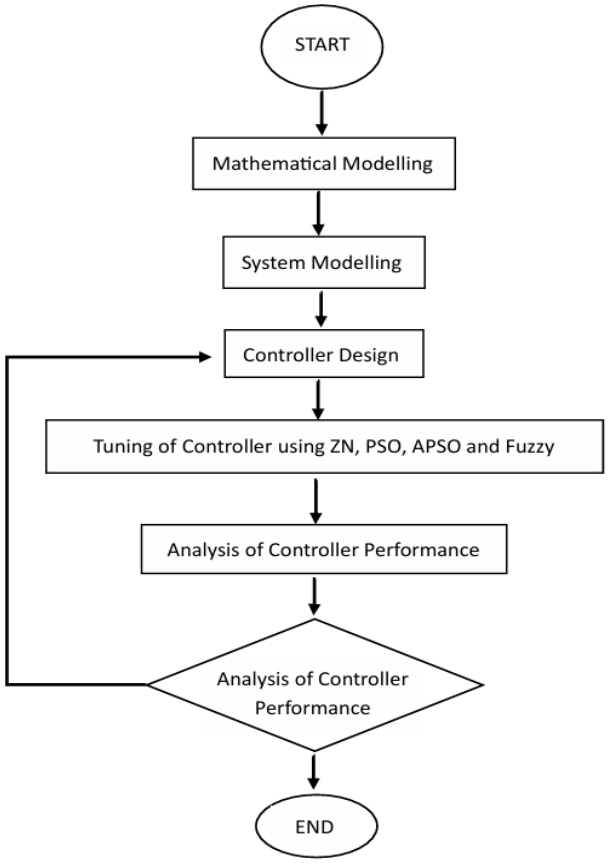

Fig. 2. The overall research methodology for EHA controller design and evaluation

The schematic diagram in Fig. 3 illustrates the pressure and flow interactions within the EHA. Here, P_s denotes the supply pressure, P_r the return pressure, and X_v the spool displacement of the valve. The chamber pressures are represented by P_1 and P_2, while Q_1 and Q_2 describe the fluid flow into and out of the two chambers. The actuator extends or retracts when there is a pressure difference $(P_1–P_2)$.

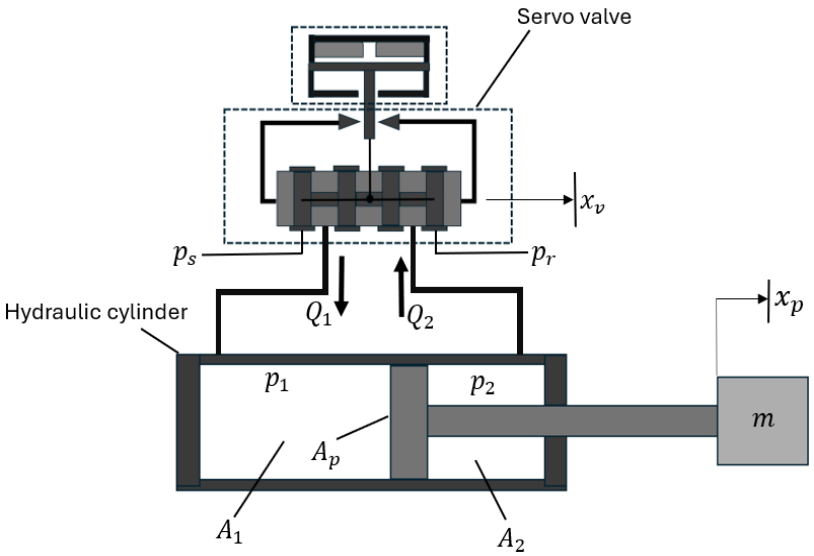

Fig. 3. The schematic diagram of EHA system

The dynamic force balance of the piston can be expressed as:

$$\dot{x}_p = SP_L - f\dot{x}_p - F_L \tag{1}$$

where m is the load mass on the piston rod, x_p the piston displacement, P_L the chamber pressure difference, k the coefficient of the elastic force, f the viscous friction coefficient, S the piston area, and F_L an external force disturbance acting on the actuator.

Assuming a high-response servo valve, the input voltage u produces a spool displacement x_V that is proportional to:

$$x_V = k_V u \tag{2}$$

where k_V is the servo valve coefficient. Since the cylinder is symmetric, the piston areas and chamber volumes are considered equal. The oil flow dynamics can therefore be described as:

$$Q_L = \dot{P}_L + \frac{2\beta S}{V}\dot{x}_P \tag{3}$$

Here, Q_L is the flow rate difference between the two chambers, V the chamber volume, and β the effective bulk modulus of the fluid. The flow relationship can also be written as:

$$Q_L = \frac{2\beta S}{V}\left[C_d w\sqrt{\frac{P_a - P_L}{\rho}}x_V - k_l P_L\right]x_l \tag{4}$$

where C_d is the discharge coefficient of the valve port, P_a the supply pressure, ρ the oil density, and k_l the leakage coefficient between the chambers. Letting Let $\dot{x}_1 = x_p$, $x_2 = \dot{x}_p$ and $x_3 = P_L$, the system dynamics can be written as:

$$\dot{x}_l = \dot{x}_p = x_2 \tag{5}$$

$$\dot{x}_2 = \ddot{x}_p \tag{6}$$

From (1),

$$\ddot{x}_p = \frac{S}{m}P_L - \frac{f}{m}\dot{x}_p - \frac{k}{m}x_p - \frac{F_L}{m} \tag{7}$$

Which simplifies to,

$$x_2 = \frac{S}{m}P_L - \frac{f}{m}\dot{x}_p - \frac{k}{m}x_p - \frac{F_L}{m} \tag{8}$$

The pressure difference dynamic can be expressed as:

$$\dot{x}_3 = \dot{P}_L \tag{9}$$

Using (3),

$$P_L = Q_L - \frac{2\beta S}{V}\dot{x}_P \tag{10}$$

Substituting (4) into (10) yields:

$$P_L = \frac{2\beta}{V}C_d w\sqrt{\frac{P_a - P_L}{\rho}}x_V - \frac{2\beta}{V}k_l P_L - \frac{2\beta}{V}\dot{x}_P \tag{11}$$

Hence, the governing differential equations for the EHA servo system under external disturbance are:

$$\dot{x}_1 = x_2 \tag{12}$$

$$\dot{x}_2 = -\frac{k}{m}x_1 - \frac{f}{m}x_2 + \frac{S}{m}x_3 - \frac{F_L}{m} \tag{13}$$

$$\dot{x}_3 = -\frac{S}{k_C}x_2 - \frac{k_l}{k_C}x_3 + \frac{C}{k_C}\sqrt{\frac{P_a - x_3}{2}}k_V u \tag{14}$$

where x_1 is the piston displacement, x_2 the piston velocity, and x_3 the differential chamber pressure $P_1 - P_2$. The disturbance force F_L may be either constant or time-varying. The physical parameters used in this model are summarized in Table 1. which are represented by (12), (13) and (14).

Table 1. Parameter of EHA servo system

No	Parameters	Symbol	Value	Units
1	Load at the EHA rod	m	0.33	Ns^2/cm
2	Piston area	S	10.0	cm^2
3	Coefficient of viscous friction	f	27.5	Ns/cm
4	Coefficient of aerodynamic elastic force	k	1000.0	N/cm
5	Valve port width	w	0.05	cm
6	Supply pressure	P_a	2100.0	N/cm^2
7	Coefficient of volumetric flow of the valve port	C_d	0.63	-
8	Coefficient of internal leakage	k_l	$2.38\text{x}10^{-3}$	cm^5/Ns
9	Coefficient of servo valve	k_V	0.017	cm/V
10	Coefficient involving bulk modulus and EHA volume	k_C	$2.5\text{x}10^{-4}$	cm^5/N
11	Oil density	ρ	$8.87\text{x}10^{-7}$	Ns^2/cm^4

By substituting all the parameters into (12), (13) and (14), the system equation can be represented in state-space form as:

$$\dot{x}(t) = Ax(t) + Bu(t) + C$$

where;

$$\dot{x}(t) = [\dot{x}_1(t) \quad \dot{x}_2(t) \quad \dot{x}_3(t)]^T$$

$$m\begin{bmatrix}\dot{x}_1\\ \dot{x}_2\\ \dot{x}_3\end{bmatrix} = \begin{bmatrix}0 & 1 & 0\\ -\frac{k}{m} & -\frac{f}{m} & \frac{S}{m}\\ 0 & -\frac{S}{k_C} & -\frac{k_l}{k_C}\end{bmatrix}\begin{bmatrix}x_1\\ x_2\\ x_3\end{bmatrix} + \begin{bmatrix}0\\ 0\\ \frac{C}{k_C}\sqrt{\frac{P_a - x_3}{2.0}}\end{bmatrix}u + \begin{bmatrix}0\\ -\frac{F_L}{m}\\ 0\end{bmatrix}$$

$$A = \begin{bmatrix}0 & 1 & 0\\ -3030.3 & -83.3 & 30.3\\ 0 & -40000.0 & -9.25\end{bmatrix}$$

$$x(t) = [x_1(t) \quad x_2(t)]^T$$

$$B = \begin{bmatrix}0 & 0 & 3196.0\sqrt{\frac{2100.0 - x_3}{2.0}}\end{bmatrix}^T$$

$$C = [0 \quad -3.03F_L \quad 0]^T$$

2.2. Controller Design and Performance Evaluation

To evaluate the performance of the EHA system, several performance indicators were chosen:

1. Overshoot ($OS\%$) - percentage overshoot in piston displacement.
2. Rise time (T_r) - time required for the piston displacement to first reach the reference value.
3. Settling time (T_s) - time for the piston displacement to remain within a defined error band of the reference.

The external force disturbance, F_L , was applied to the actuator to test the robustness of the controllers. Four disturbance cases were considered:

1. Case 1: F_L= 0 N
2. Case 2: F_L= 1000 N
3. Case 3: F_L= 5000 N
4. Case 4: F_L= 10000 N

2.2.1. PID Controller Designed Using Ziegler-Nichols (ZN-PID) Method

A conventional PID controller structure is employed due to its well-established theoretical foundation and practical relevance in industrial control applications. The Ziegler–Nichols method, originally developed in the 1940s by J.G. Ziegler and N.B. Nichols, is among the most widely recognized and applied approaches for PID parameter tuning. It relies on a closed-loop experimental procedure to estimate controller gains [38]-[43]. In this study, the Ziegler–Nichols tuning method is employed as a baseline approach due to its simplicity and extensive industrial adoption, providing a reference point for comparative performance evaluation.

In this approach, the integral K_I and derivative K_D actions are set to zero, and only the proportional gain K_P, is gradually increased. As K_P, rises, the system eventually reaches a point of sustained oscillation with constant amplitude. At this point, the corresponding proportional gain is referred to as the ultimate gain K_U, while the oscillation period is called the ultimate period P_U. Once K_U and P_U are obtained, the PID gains are calculated using the Ziegler–Nichols tuning rules provided in Table 2. These formulas determine the values of K_P, K_I and K_D needed for controller implementation.The block diagram of the EHA system integrated with a PID controller is shown in Fig. 4, where the gains are set according to the ZN method.

2.2.2. PID Controller Designed Using Particle Swarm Optimization (PSO-PID) Technique

Swarm Optimization (PSO), first introduced by Kennedy and Eberhart in 1995, is an optimization algorithm inspired by the collective behavior of animals such as birds flocking or fish schooling. The main concept is that a population of candidate solutions, known as particles, moves within the search space to locate the optimal solution [44]-[49]. In this study, Particle Swarm Optimization is employed to automatically search for optimal PID gains by minimizing the tracking error, thereby overcoming the limitations of manual tuning under uncertain and disturbance-prone operating conditions. Each particle updates its position using two pieces of knowledge:

1. Its own personal best position, P_{Best} found so far.
2. The global best position, G_{Best} identified by the entire swarm.

Table 2. ZN method to obtain PID controller parameter

Controller	K_P	K_I	K_D
PID Value	$0.6 * K_U$	$2.0 * K_U/K_P$	$K_U * P_U/8.0$

The particle's position and velocity are updated iteratively according to the following relations:

$$x^{i+1} = x^i + v^{i+1} \tag{15}$$

$$v^{i+1} = \omega v^i + c_1 r_1 \left(P_{Best} - x^i\right) + c_2 r_2 \left(G_{Best} - x^i\right) \tag{16}$$

where ω is inertia factor, c_1 and c_2 are acceleration coefficient, while r_1 and r_2 are random values between 0 and 1.

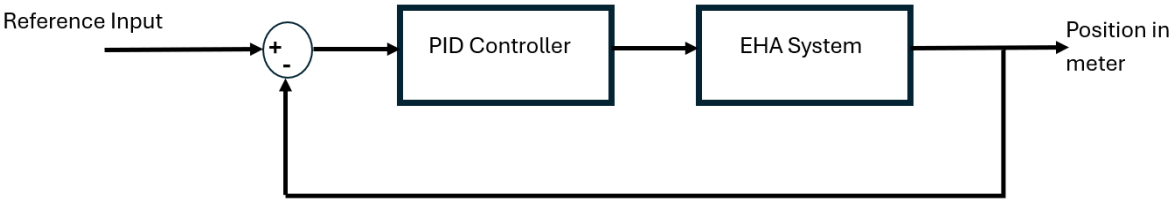

Fig. 4. The EHA system block diagram with PID controller

In this work, the optimization task is formulated as a three-dimensional problem in which the PSO algorithm searches for the best set of PID gains (K_P,K_I and K_D). The selected parameters for the PSO procedure are:

- Number of particles: 25
- Search space dimension: 3 (for K_P,K_I and K_D)
- Maximum iterations: 50

The optimization was carried out incrementally, beginning with 5 particles and 10 iterations, then gradually increasing to 25 particles and 50 iterations. This progressive approach allows the swarm to refine its search and converge toward an optimal solution. The selection of 25 particles and 50 iterations was based on a convergence–computational trade-off study. The optimization was initially executed with smaller swarm sizes and iteration numbers and then progressively increased. It was observed that the fitness value (SSE) converged consistently before reaching the maximum iteration limit, as evidenced by the stabilization of SSE values shown in Table 3, Table 4, Table 5, Table 6. Increasing the number of particles or iterations beyond these values did not yield significant improvement in performance, indicating that the chosen parameters were sufficient to ensure convergence while maintaining computational efficiency.

The fitness function used is the Sum of Squared Errors (SSE), where lower values indicate better tracking performance. The best fitness value in each optimization cycle corresponds to the optimal set of PID gains. The Table 3, Table 4, Table 5, Table 6. summarize the SSE results obtained under external disturbances of 0N, 1000N, 5000N, and 10000 N. For each external disturbance case, the PID gains were independently optimized using the same PSO configuration and objective function. The gains reported correspond to the optimal solution that minimizes the SSE for the specific disturbance level, ensuring a fair and consistent comparison across all cases. The overall procedure of the PSO algorithm applied is illustrated in the flowchart in Fig. 5.

The value of SSE when F_L = 0N is tabulated in Table 3. From the table, the smallest SSE value recorded is 1.2479 at 20 particles, 40^{th} iteration. The value of SSE when F_L = 1000N is recorded in Table 4. From the table, the smallest SSE value is 1.1961 at 25 particles, 50^{th} iteration. The value of SSE when F_L = 5000N is recorded in Table 5. From the table, the smallest SSE value is 1.2431 at 25 particles, 50^{th} iteration. The value of SSE when F_L = 10000N is recorded in Table 6. Table 5 From the table, the smallest SSE value is 1.4219 at 25 particles, 50^{th} iteration.

2.2.3. PID Controller Designed Using Adaptive Particle Swarm Optimization (APSO-PID) Method

In the APSO-PID approach, the optimized PID gains obtained from the PSO procedure under each disturbance level are used to construct a gain lookup table, enabling adaptive gain selection

based on the detected external force. Adaptive Particle Swarm Optimization is adopted to enhance tuning robustness by dynamically adjusting swarm parameters, allowing improved convergence behavior and adaptability when system dynamics vary due to mismatched conditions. The Table 7. shows the associated PID gains corresponding to specific levels of external disturbance, F_L. The lookup table serves as a reference for the adaptive PSO controller, enabling it to adjust the PID gains dynamically based on the detected disturbance level [50]-[54].

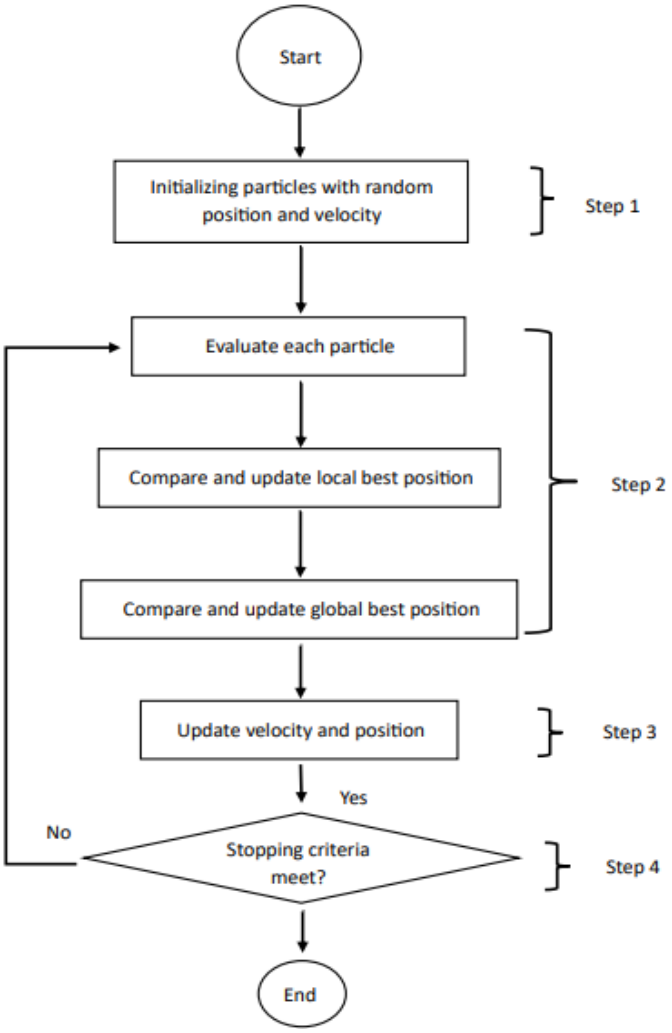

Fig. 5. The flowchart of PSO technique [22]

Table 3. SSE values when $F_L = 0N$

N_p/N_i	5	10	15	20	25
10	4.5605	4.7302	5.6756	2.3644	3.7789
20	3.3582	2.4032	3.3360	2.1706	1.9042
30	1.8971	3.9462	1.7921	1.6653	1.7434
40	3.2942	2.2429	1.4942	**1.2479***	1.3920
50	2.6841	1.8527	1.3735	1.7059	1.7197

Table 4. SSE values when $F_L = 1000N$

N_p/N_i	5	10	15	20	25
10	6.3611	2.7241	3.4637	2.6617	4.3038
20	3.3939	3.9745	1.5016	1.8982	1.6350
30	2.0555	5.4835	1.2003	3.0403	1.5339
40	3.6487	1.6804	2.1598	2.0913	2.3262
50	2.2745	2.2428	1.2011	1.4057	**1.1961***

Table 5. SSE values when F_L= 5000N

N_p/N_i	5	10	15	20	25
10	8.8735	3.4483	4.5641	4.5263	2.6964
20	3.4869	3.0351	1.4097	1.3136	1.3112
30	2.0721	1.8641	2.9953	2.2268	1.2915
40	1.3135	5.4313	1.8268	1.2922	1.2927
50	1.2906	1.3616	1.2905	1.2913	**1.2431***

Table 6. SSE values when F_L= 10000N

N_p/N_i	5	10	15	20	25
10	2.5603	8.2872	3.1959	5.6882	17.7677
20	6.4800	4.2938	3.4205	1.4425	2.1703
30	1.7035	6.8087	5.2506	2.2565	1.8723
40	2.6341	1.8431	1.3368	1.5856	2.4311
50	1.8042	2.5550	2.0404	1.4238	**1.4219***

Table 7. Adaptive PSO-PID look-up table

Gain Value	External Disturbance, F_L			
	0 N	1000 N	5000 N	10000 N
K_P	K_P Value 1	K_P Value 2	K_P Value 3	K_P Value 4
K_I	K_I Value 1	K_I Value 2	K_I Value 3	K_I Value 4
K_D	K_D Value 1	K_D Value 2	K_D Value 3	K_D Value 4

The function takes F_L as input and determines the appropriate PID gains K_P, K_I, and K_D using a series of if-elseif-else statements. Specific gain values are defined for four disturbance levels. The calculated gains are then used to update the PID controller in real-time.

2.2.4. PID Controller Designed Using Fuzzy (FPID) Method

Conventional PID controllers are widely employed in industry to regulate process variables such as displacement, force, or pressure. Their main task is to ensure that the system output follows the reference signal as closely as possible by adjusting the control input through feedback. However, because the PID gains are fixed, their performance tends to deteriorate when the system operates under varying conditions [55]-[60]. The Fuzzy-PID controller is introduced to enhance robustness against nonlinearities and uncertainties by incorporating fuzzy logic–based gain adjustment, enabling improved tracking performance under varying disturbance levels.

To address this limitation, a Fuzzy-PID (FPID) controller is designed. This approach integrates fuzzy logic with the PID structure so that the controller gains (K_P, K_I, and K_D) can be tuned adaptively in real time. The fuzzy tuner adjusts the parameters based on the external disturbance, F_L allowing the controller to maintain robustness and accuracy under different operating scenarios. The FPID framework is illustrated in Fig. 6. In this setup, the disturbance signal is passed to fuzzy inference modules that generate adaptive values for K_P, K_I, and K_D. To represent the disturbance input, triangular membership functions are defined, as shown in Fig. 7. The five input states are classified as Very Small (VS), Small (S), Medium (M), Big (B), and Very Big (VB).

The ranges of the fuzzy membership functions were selected based on the expected operating limits of the external disturbance and the corresponding PID gain values observed during PSO optimization. Preliminary simulation trials were conducted to ensure that the selected ranges provided sufficient sensitivity to disturbance variations while avoiding saturation effects. Triangular membership functions were chosen due to their simplicity, smooth interpolation characteristics, and widespread use in real-time fuzzy control applications. The outputs of the fuzzy tuners are mapped within specific where K_P, outputs having ranges from 80.0 to 150.0, K_I outputs having ranges from 25.0 to 130.0 and K_D ranges from -0.06 to 0.02. The membership functions for these three outputs are presented in Fig. 8, Fig. 9 and Fig. 10 respectively. A set of fuzzy inference rules links the disturbance magnitude to the adjustment of each gain. These rules, summarized in Table 8, define

how F_L influences the values of K_P, K_I and K_D. The fuzzy outputs from all rules are aggregated and then converted into crisp values using the centroid defuzzification technique. The resulting gain values are applied directly to the PID controller, enabling adaptive tuning. To maintain a fair comparison, the fuzzy membership functions and rule base were kept fixed throughout the study, while the controller performance was evaluated under varying disturbance conditions.

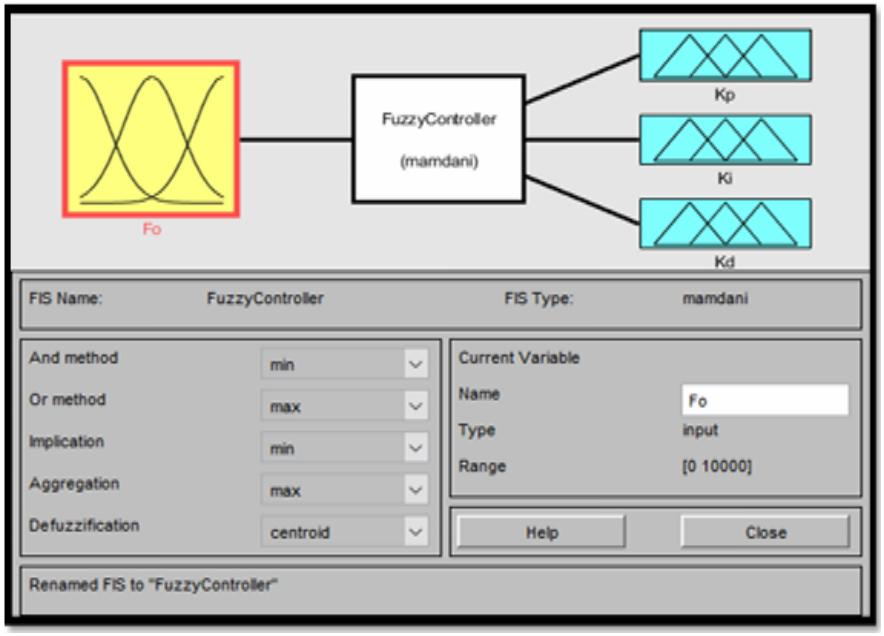

Fig. 6. The fuzzy logic designer

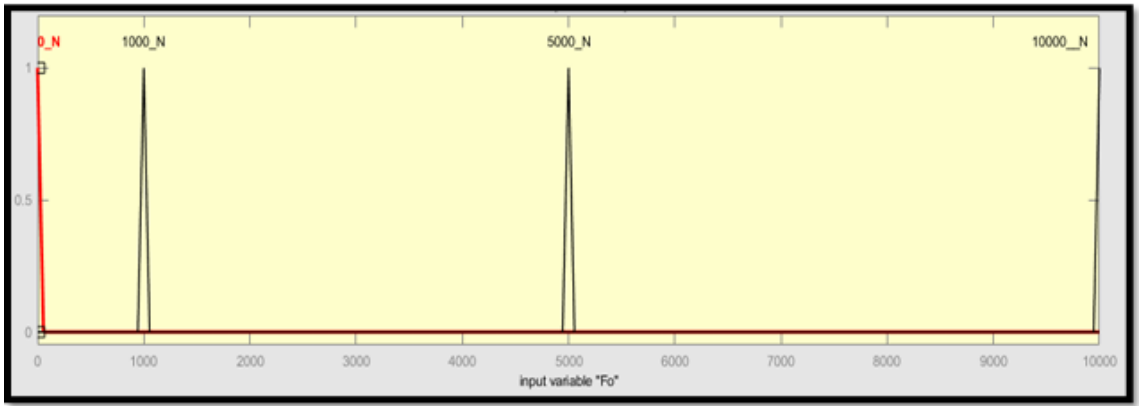

Fig. 7. The membership function of input F_L

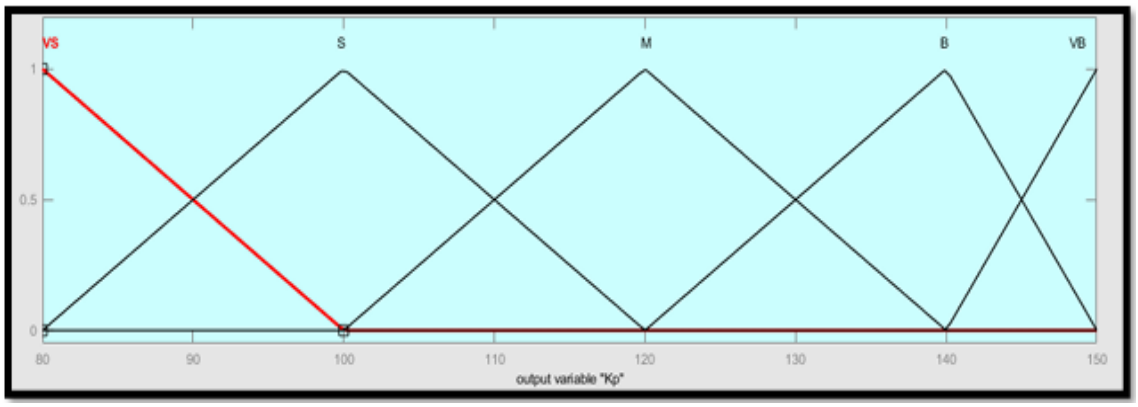

Fig. 8. The membership function of output K_P

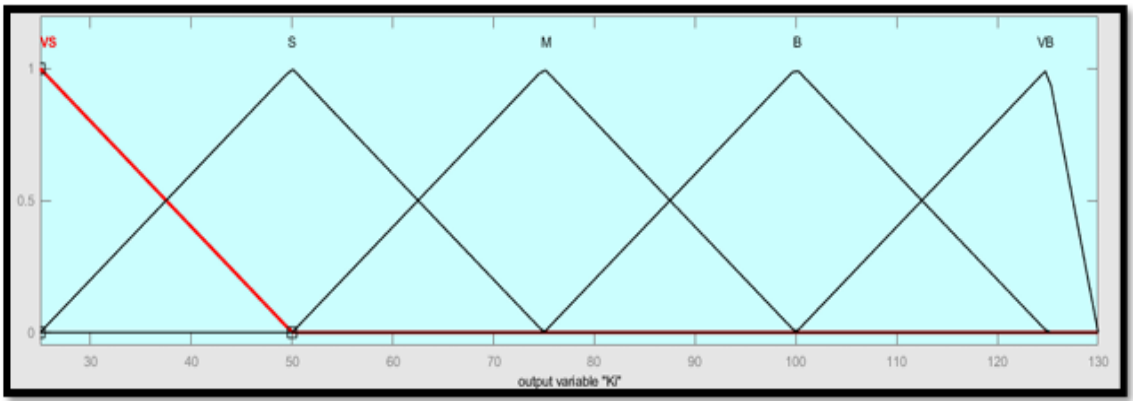

Fig. 9. The membership function of output K_I

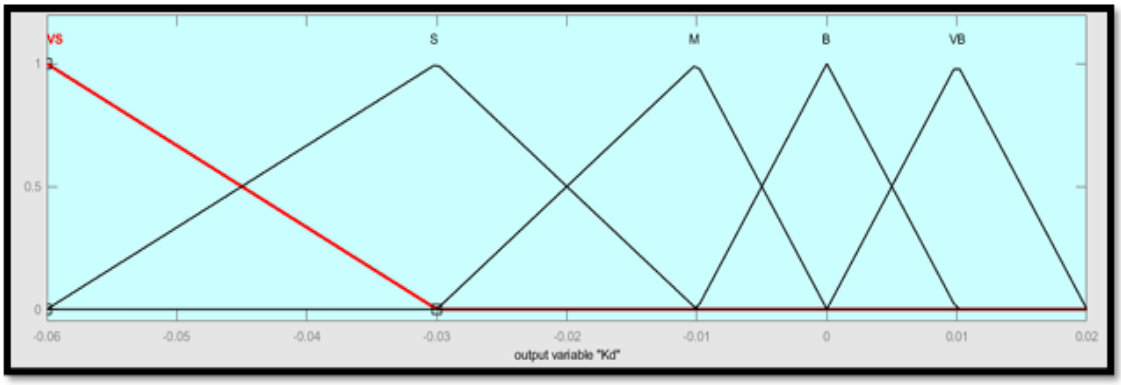

Fig. 10. The membership function of output K_D

Table 8. Fuzzy rule table of the fuzzy tuners of FPID

External Disturbance, F_L	Gain Values		
	K_P	K_I	K_D
0 N	VS	VS	M
1000 N	S	S	VS
5000 N	M	M	VS
10000 N	VB	VB	VS

2.2.5. MATLAB Simulink Model of the EHA System

The EHA system's equation is inserted into the MATLAB simulator, and the system's block diagram is drawn in the MATLAB Simulink (simulator). The signal flow graph is constructed using the state-space equation after obtaining the EHA system equation. After constructing the signal flow graph, it is then inserted into the EHA system's functional block known as the array block. The EHA system model is then simulated to observe the system's performance. Fig. 11 shows the block structure constructed using the signal flow graph which makes up the EHA system while Fig. 12 shows the complete block structure of EHA system with PID controller built in MATLAB.

2.2.6. Reference Trajectory Test

A square wave signal as shown in Fig. 13 is used as the reference trajectory for the EHA system. The PID controller is designed to help track the signal resulting in lower tracking error. The EHA system output must follow the reference signal via the help designed PID controller combined with ZN-PID, PSO-PID, APSO-PID and FPID tuning method under four cases of external disturbances. The purpose of this square wave signal is to show the intended controller's ability to assist the system in tracking the path point by point trajectory.

To accurately analyze the performance and robustness of the EHA system under realistic operational conditions, it is crucial to simulate the varying external forces the EHA may encounter

in its intended application. A custom external disturbance signal was designed and implemented using Simulink's Signal Builder block to achieve this goal as shown in Fig. 14. This custom signal aims to replicate the represents the varying dynamic and unpredictable nature of real-world external disturbances that could act on the EHA system over a 10-second time frame and check the adaptability of the APSO-PID and FPID controller.

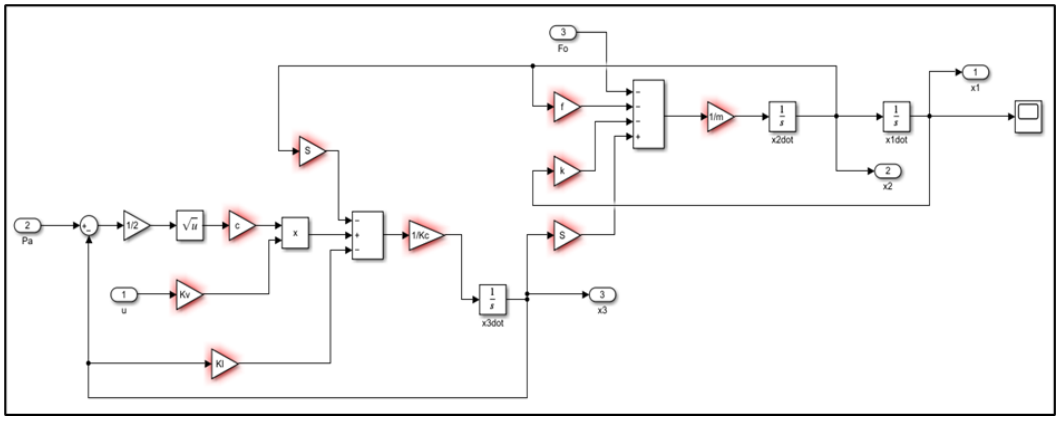

Fig. 11. The block structure of EHA system in Simulink

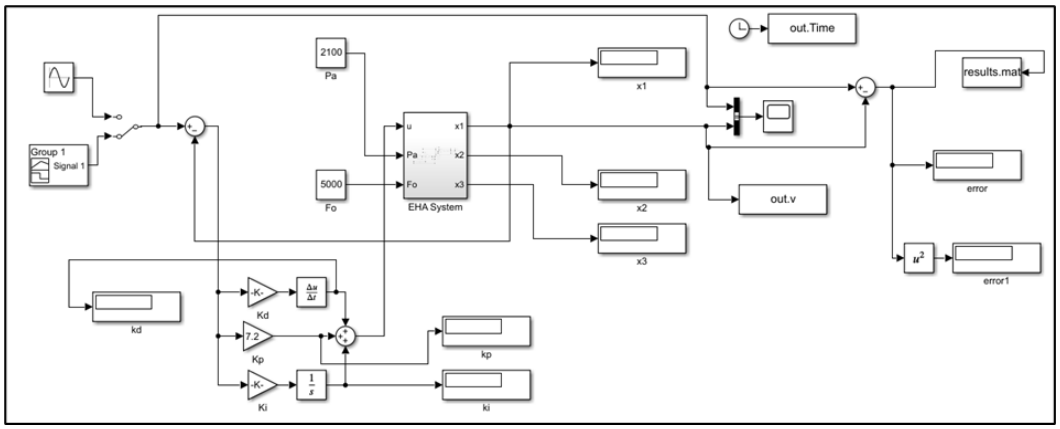

Fig. 12. The EHA system with PID controller

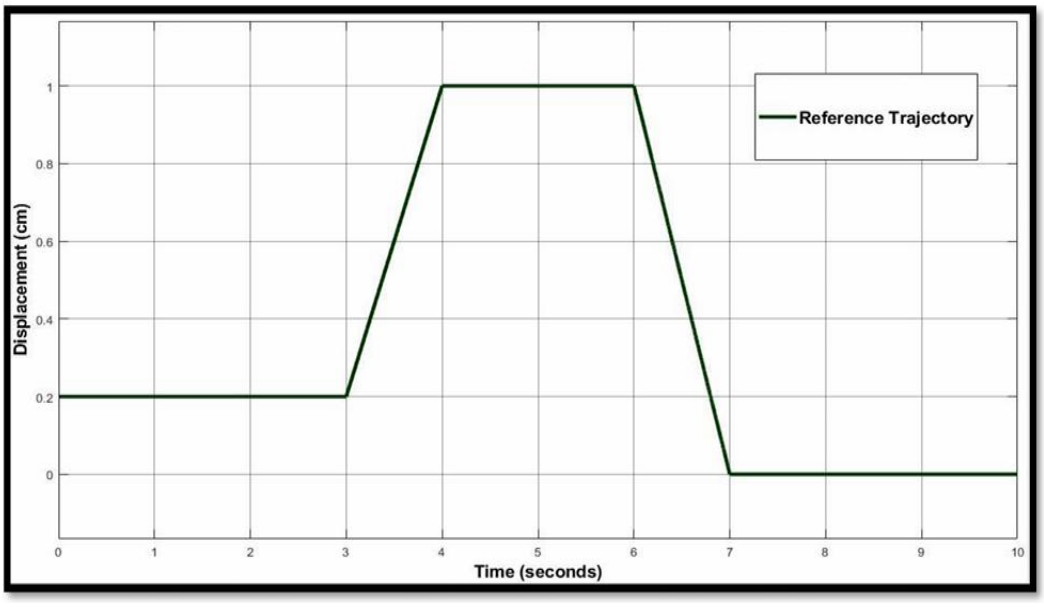

Fig. 13. The reference trajectory square wave signal

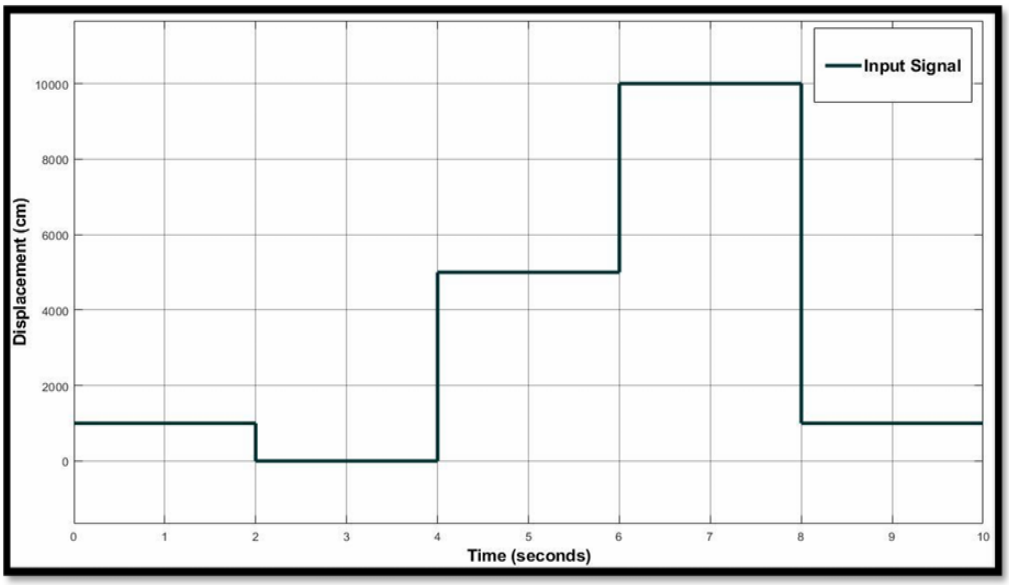

Fig. 14. The input signal for varying external disturbance

Classical transient performance indices such as rise time, settling time, and overshoot were evaluated using step input responses to ensure consistency with their standard control-theoretic definitions. For trajectory tracking analysis under square-wave reference signals with smooth transitions, controller performance was primarily assessed using steady-state error and the sum of squared error (SSE). This separation ensures that each performance metric is applied under appropriate reference conditions, thereby maintaining methodological rigor and enabling a fair comparison among the different PID tuning strategies.

3. Result and Discussion

The performance of the proposed controllers was carried out through MATLAB Simulink simulations. The ZN-PID, PSO-PID, APSO-PID, and FPID methods were compared to assess their tracking performance and robustness under different external disturbance conditions. Classical transient performance indices such as rise time, overshoot, and settling time are evaluated using isolated step input responses, where these metrics are well defined. For trajectory tracking analysis under square-wave reference signals with smooth transitions, controller performance is primarily assessed using steady-state error and sum of squared error (SSE). This separation ensures that each performance metric is applied under appropriate reference conditions.

3.1. PID Gain Values Obtained Via Four Optimization Methods

The PID gain values of these methods had tabulated in Table 9, Table 10, Table 11, and Table 12. for external disturbance, F_L of 0N, 1000N, 5000N and 10000N respectively.

Table 9. PID gain when F_L= 0N

Gain Values	ZN-PID	PSO-PID	APSO-PID	FPID
K_P	9.0000	81.1569	81.2000	86.4000
K_I	261.3400	27.6801	27.9000	33.0000
K_D	0.0775	0.0108	0.0100	-0.0133

Table 10. PID gain when F_L= 1000N

Gain Values	ZN-PID	PSO-PID	APSO-PID	FPID
K_P	8.6400	112.2649	112.2649	100.0000
K_I	264.8200	32.8865	32.8865	50.0000
K_D	0.0713	-0.0548	--0.0548	-0.0503

Table 11. PID gain when F_L= 5000N

Gain Values	ZN-PID	PSO-PID	APSO-PID	FPID
K_P	7.2000	124.2160	124.2160	120.0000
K_I	278.7600	83.6955	83.6955	75.0000
K_D	0.0465	-0.0049	-0.0049	-0.0503

Table 12. PID gain when F_L= 10000N

Gain Values	ZN-PID	PSO-PID	APSO-PID	FPID
K_P	7.8000	147.8352	147.8352	147.0000
K_I	279.8400	127.6761	127.6761	118.0000
K_D	0.0545	-0.0011	-0.001	-0.0503

3.2. Graphical Comparisons Between 4 Cases of F_L

For graphical comparison, the transient response of the EHA system when it is tuned with ZN-PID, PSO-PID, APSO-PID and FPID method is compared with the reference trajectory for total period of 10 second where, Section A is from 0 sec to 3 sec, Section B from 4 to 6 sec and finally Section C from 7 to 10 sec.

3.2.1. Comparison on Transient Response When F_L = 0N

The Fig. 15, Fig. 16, Fig. 17, Fig. 18 shows how the conventional PID, PSO-PID, APSO-PID, and FPID controllers respond when a 0 N external disturbance is injected to the EHA system. To better highlight the differences in performance Table 13, Table 14 and Table 15 breaks down and compares each controller's behavior in detail, dividing the transient response into three clear sections.

Table 13. Transient response analysis for step input reference signal for section A when F_L= 0N

Gain Values	ZN-PID	PSO-PID	APSO-PID	FPID
Settling Time (s)	1.1339	0.0024	2.9993	0.0595
Overshoot (OS%)	33.3300	-	-	-
Steady-state Error	$0.0005e^{-3}$	$0.2489e^{-3}$	-	0.0003
Rise Time (s)	0.0737	0.0316	0.0049	0.0295

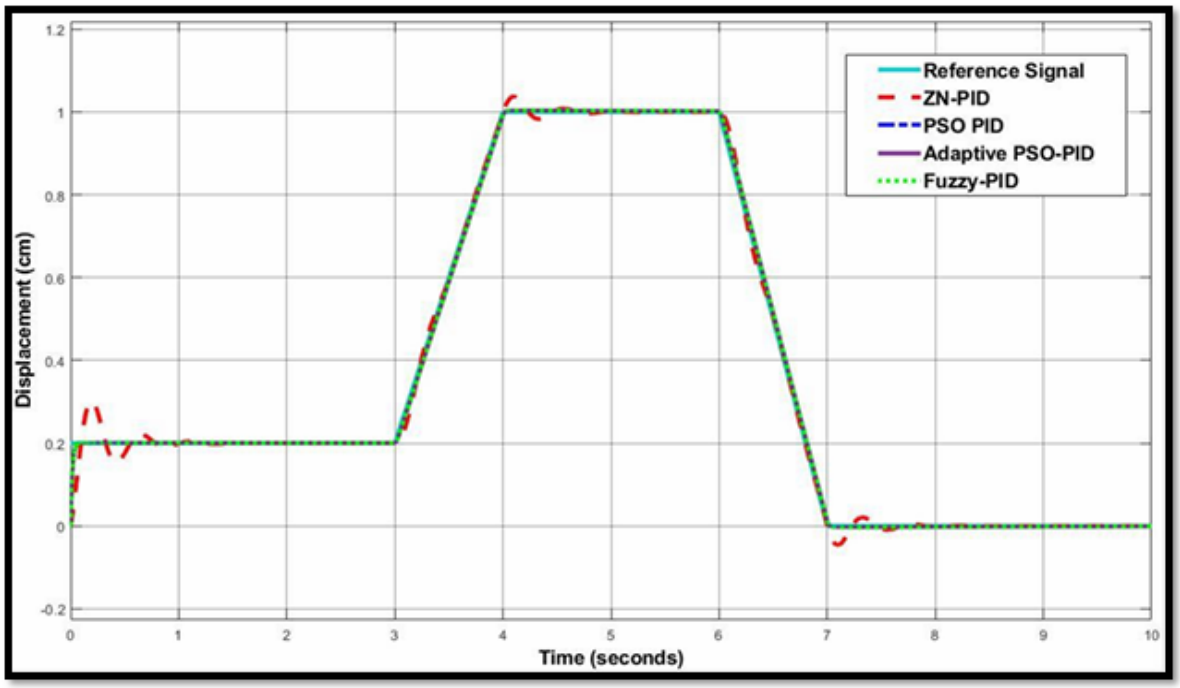

Fig. 15. The comparison between 4 methods when F_L= 0N

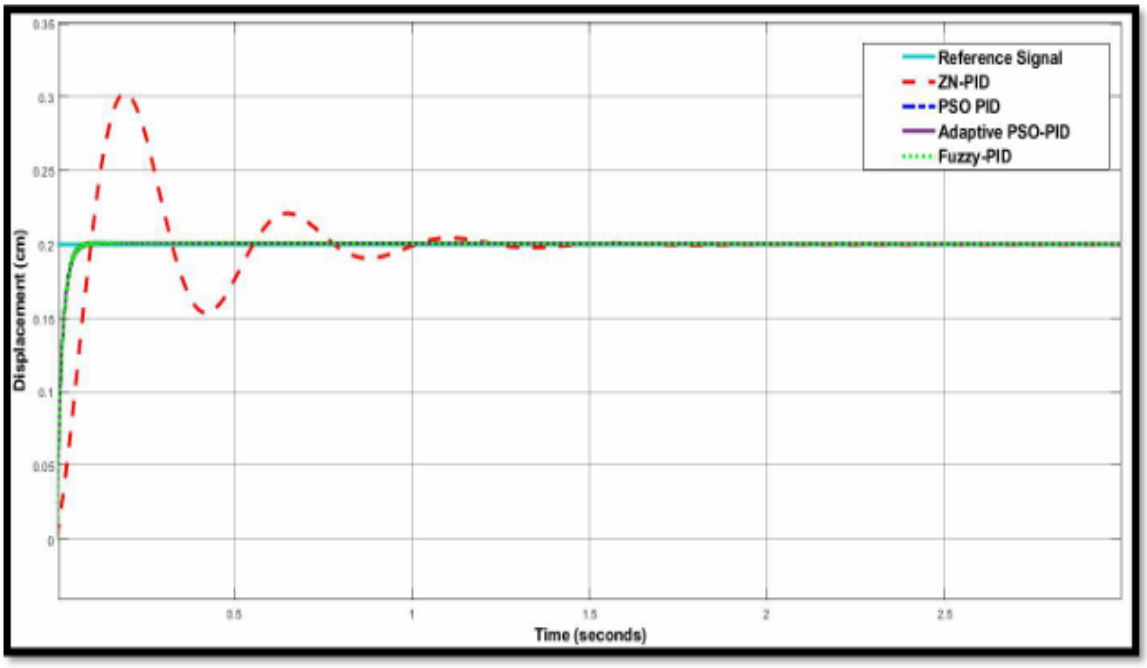

Fig. 16. The comparison between 4 methods for section A when F_L= 0N

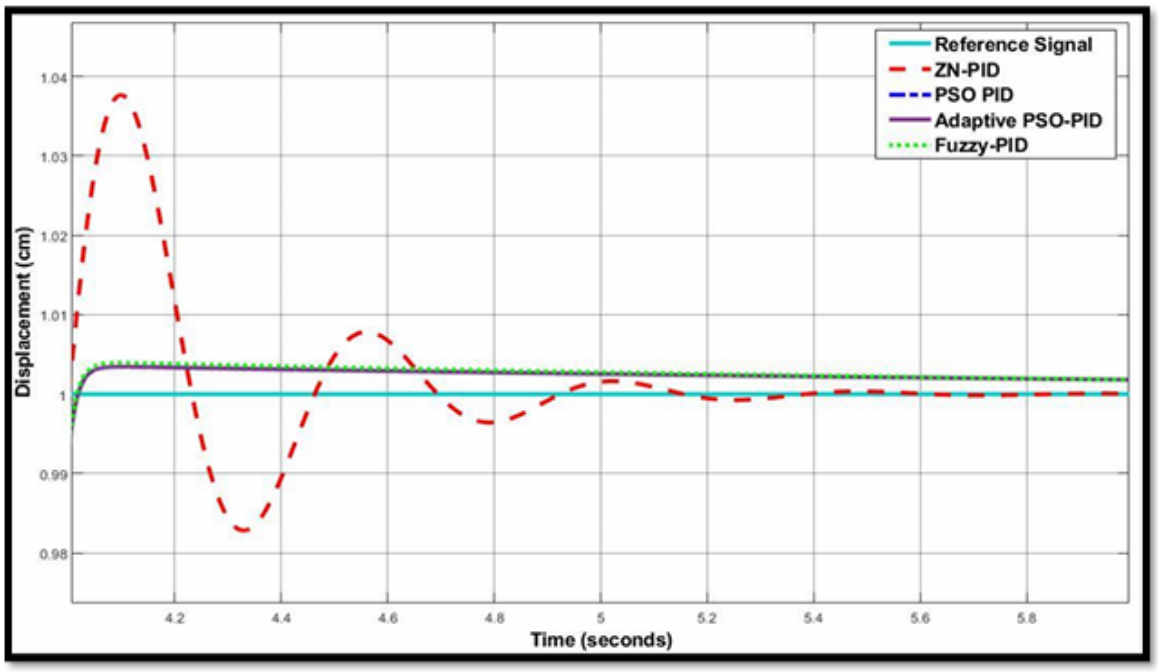

Fig. 17. The comparison between 4 methods for section B when F_L= 0N

Table 14. Transient response analysis for step input reference signal for section B when F_L= 0N

Gain Values	ZN-PID	PSO-PID	APSO-PID	FPID
Settling Time (s)	4.1700	4.0590	5.6460	4.1760
Overshoot (OS%)	3.6600	-	0.5000	-
Steady-state Error	$0.0523e^{-3}$	$1.249e^{-3}$	0.0030	0.0014
Rise Time (s)	0.0670	0.0300	0.0310	0.0240

At Section A, PSO-PID and FPID quickly settle around the target, faster than ZN-PID and APSO-PID. ZN-PID overshoots the target, while the others respond more smoothly. All controllers

stay close to the target after settling, with ZN-PID and FPID being the most accurate. APSO-PID reacts the fastest, followed closely by PSO-PID and FPID. In Section B, all four controllers settle at about the same speed. PSO-PID and FPID stand out for having no overshoot, while ZN-PID and APSO-PID have small ones. PSO-PID reacts the fastest but ends up being the least accurate. FPID finds a good balance as it reacts quickly and stays close to the target. At Section C, ZN-PID and APSO-PID overshoot a little, while PSO-PID and FPID smoothly reach the target. PSO-PID and FPID are the most accurate after settling. ZN-PID is slightly off, and APSO-PID is the least accurate. ZN-PID is also the slowest to start reacting-the others respond too fast to measure accurately.

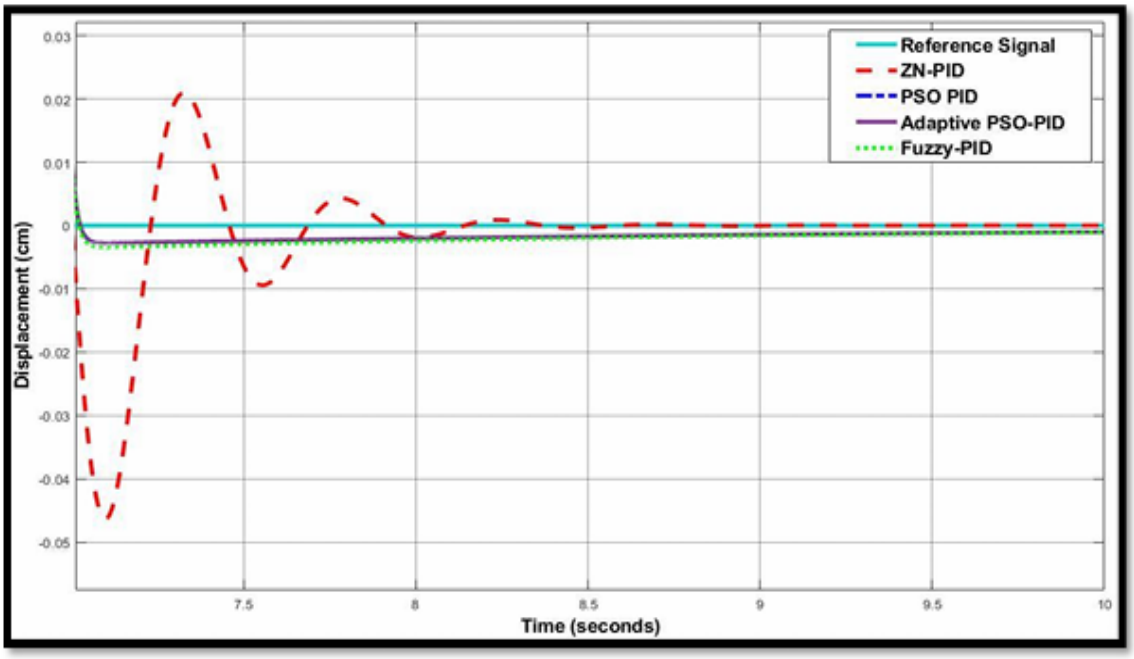

Fig. 18. The comparison between 4 methods for section C when F_L= 0N

Table 15. Transient response analysis for step input reference signal for section C when F_L= 0N

Gain Values	ZN-PID	PSO-PID	APSO-PID	FPID
Settling Time (s)	7.3370	7.0160	7.1190	7.2250
Overshoot (OS%)	1.0000	-		-
Steady-state Error	$0.0007e^{-3}$	$0.5727e^{-3}$	0.0010	0.0008
Rise Time (s)	0.2110	-	-	-

3.2.2. Comparison on Transient Response When F_L = 1000N

The Fig. 19, Fig. 20, Fig. 21, Fig. 22 shows how the conventional PID, PSO-PID, APSO-PID, and FPID controllers respond when a 1000 N external disturbance is injected into the EHA system. To better highlight the differences in performance, Table 16, Table 17 and Table 18 breaks down and compares each controller's behavior in detail, dividing the transient response into three clear sections.

At Section A, FPID and PSO-PID settle the fastest, meaning they quickly reach the target. ZN-PID and APSO-PID take longer to settle. ZN-PID and PSO-PID both overshoot the target a bit, while FPID and APSO-PID stay smooth with no overshoot. All four controllers stay close to the target in the end, but FPID is the most accurate. APSO-PID reacts the quickest, followed by FPID and PSO-PID. ZN-PID is the slowest to react. In Section B, ZN-PID again shows a big overshoot. FPID and APSO-PID are the most accurate, with very small steady-state errors. ZN-PID is close behind, while PSO-PID has the biggest final error. PSO-PID reacts fastest, and FPID also responds quickly. ZN-PID and APSO-PID take longer to react. At Section C, all four controllers settle at about the same speed. ZN-PID and APSO-PID show a small overshoot. PSO-PID and FPID reach the target smoothly. PSO-PID and FPID are the most accurate at the end, ZN-PID is slightly off, and APSO-

PID is the least accurate. ZN-PID reacts the slowest, while the others respond too fast to clearly measure. Overall, FPID performs the best as it reacts quickly, doesn't overshoot, and stays closest to the target. PSO-PID is the fastest to respond, but its accuracy could be better.

Table 16. Transient response analysis for step input reference signal for section A when F_L= 1000N

Gain Values	ZN-PID	PSO-PID	APSO-PID	FPID
Settling Time (s)	1.1634	0.0210	3.0000	0.0601
Overshoot (OS%)	34.8500	3.6460	1.0000	-
Steady-state Error	$0.0094e^{-3}$	$0.1459e^{-3}$	$0.0947e^{-3}$	0.0002
Rise Time (s)	0.0736	0.0202	$1.5900e^{-3}$	0.0245

Table 17. Transient response analysis for step input reference signal for section B when F_L= 1000N

Gain Values	ZN-PID	PSO-PID	APSO-PID	FPID
Settling Time (s)	4.1800	4.2110	4.2850	4.1690
Overshoot (OS%)	3.7500	-	-	0.5000
Steady-state Error	$0.0977e^{-3}$	$1.474e^{-3}$	1.0000	0.0015
Rise Time (s)	0.0750	0.0370	0.0700	0.0320

Table 18. Transient response analysis for step input reference signal for section C when F_L= 1000N

Gain Values	ZN-PID	PSO-PID	APSO-PID	FPID
Settling Time (s)	7.3580	8.9350	7.7090	8.5580
Overshoot (OS%)	1.0000	-	1.0500	-
Steady-state Error	$-0.0002e^{-4}$	0.0007	0.0007	0.0006
Rise Time (s)	0.0720	-	-	-

3.2.3. Comparison on Transient Response When F_L = 5000N

The Fig. 23, Fig. 24, Fig. 25, Fig. 26 shows how the conventional PID, PSO-PID, APSO-PID, and FPID controllers respond when a 5000 N external disturbance is injected to the EHA system. To better highlight the differences in performance, Table 19, Table 20 and Table 21 breaks down and compares each controller's behavior in detail, dividing the transient response into three clear sections.

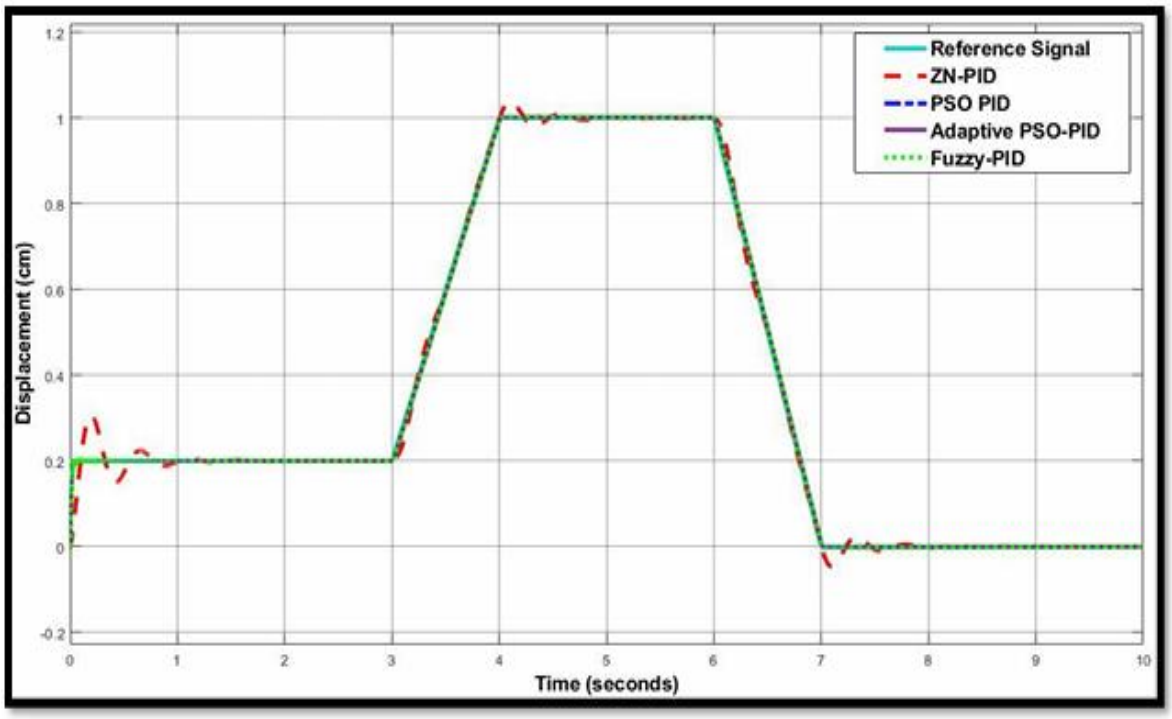

Fig. 19. The comparison between 4 methods when F_L= 1000N

Table 19. Transient response analysis for step input reference signal for section A when F_L= 5000N

Gain Values	ZN-PID	PSO-PID	APSO-PID	FPID
Settling Time (s)	1.4349	0.0600	3.0000	0.0651
Overshoot (OS%)	38.8400	1.0000	1.0000	1.0000
Steady-state Error	$0.123e^{-3}$	$0.0315e^{-3}$	0.0010	$0.0203e^{-5}$
Rise Time (s)	0.0741	0.0300	0.0053	0.0240

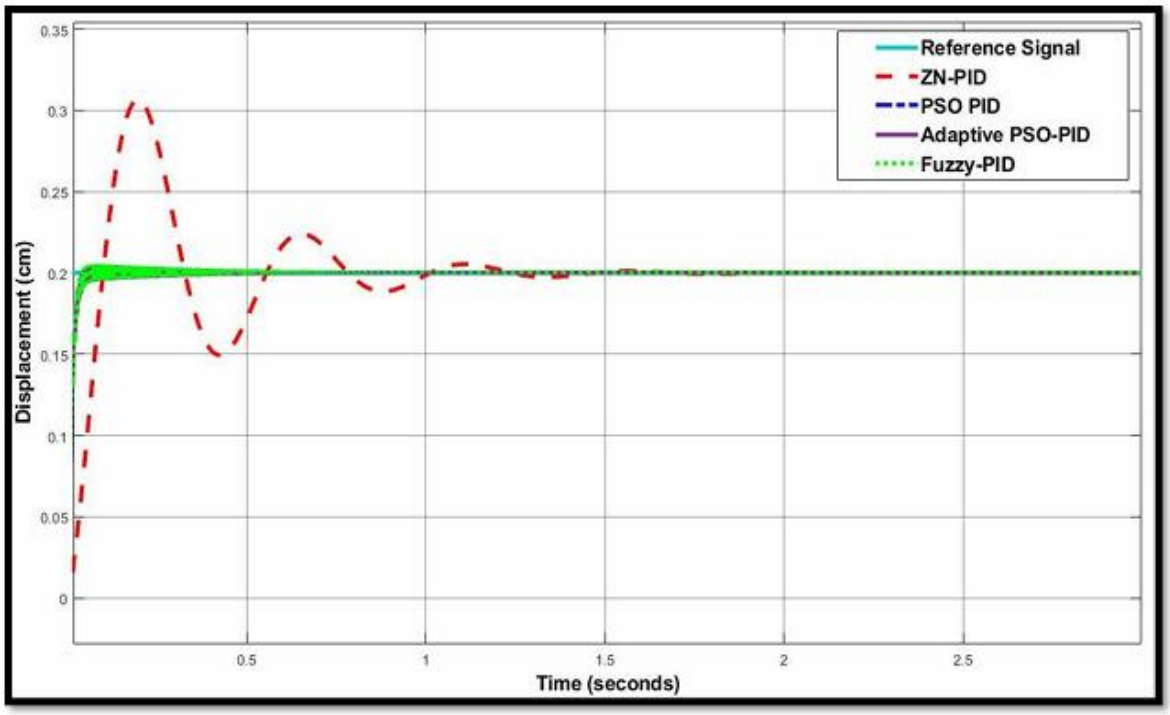

Fig. 20. The comparison between 4 methods for section A when F_L= 1000N

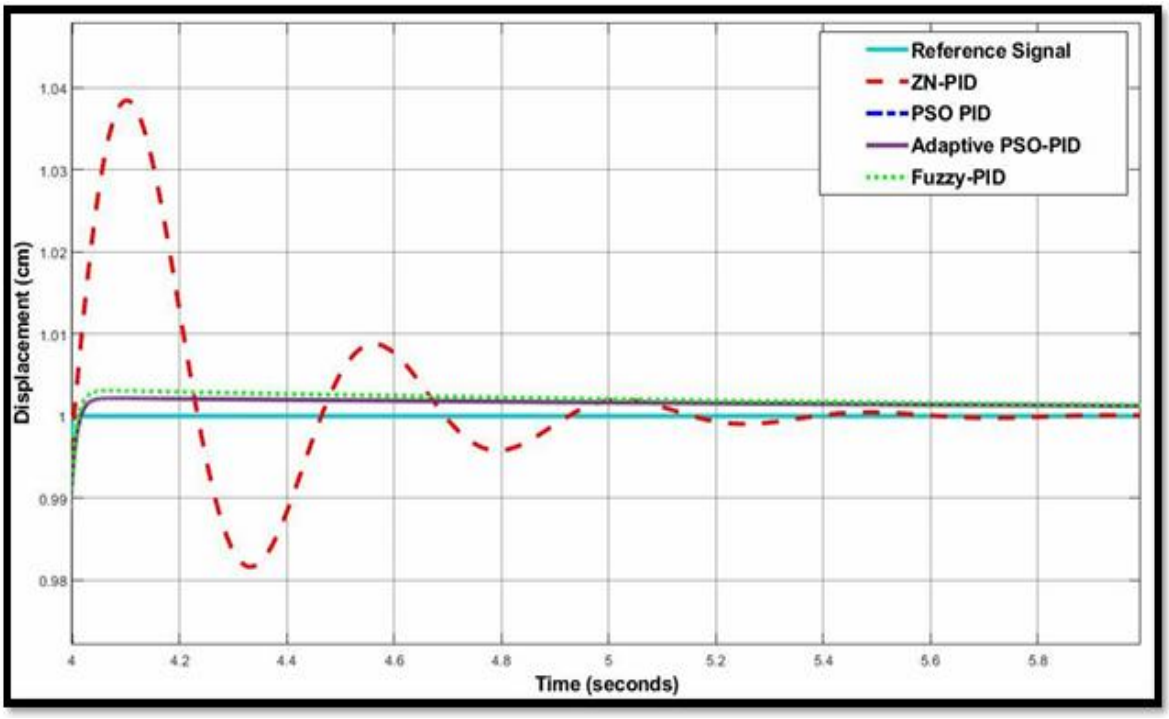

Fig. 21. The comparison between 4 methods for section B when F_L= 1000N

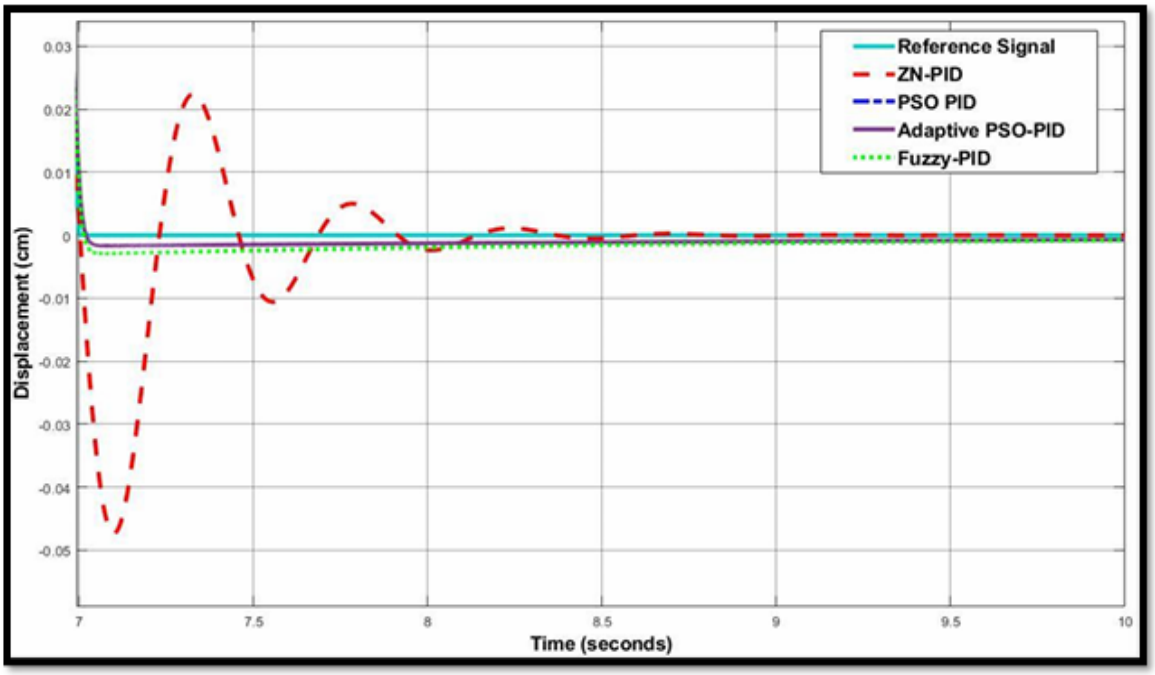

Fig. 22. The comparison between 4 methods for section C when F_L= 1000N

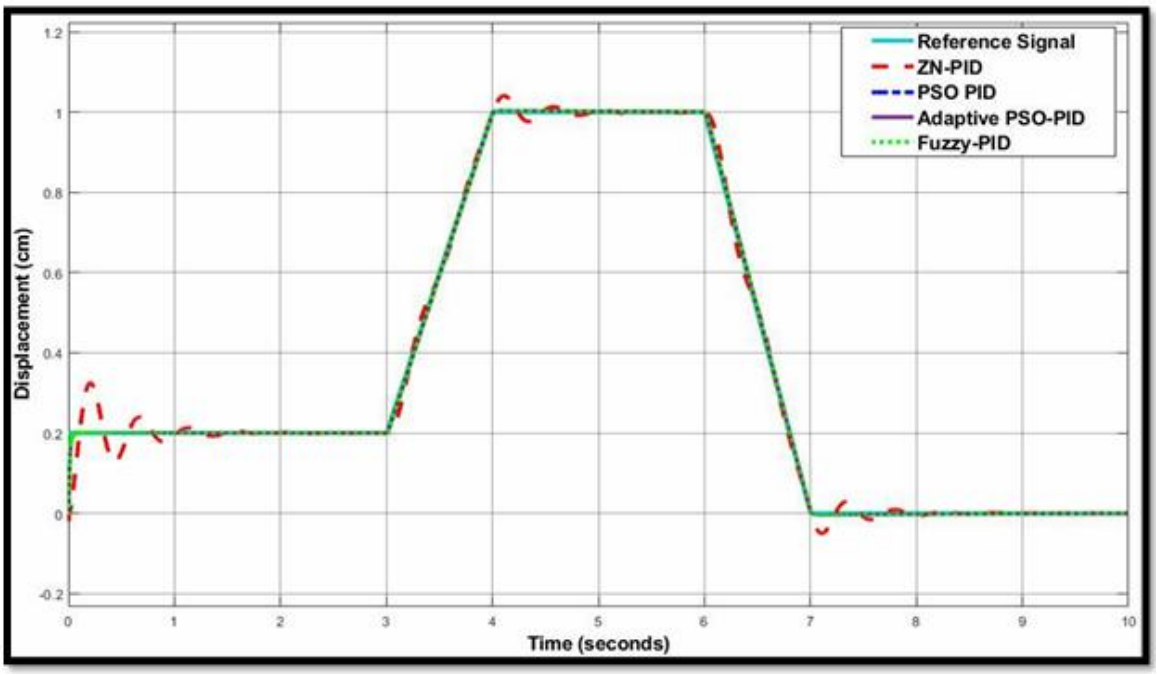

Fig. 23. The comparison between 4 methods when F_L= 5000N

Table 20. Transient response analysis for step input reference signal for section B when F_L= 5000N

Gain Values	ZN-PID	PSO-PID	APSO-PID	FPID
Settling Time (s)	4.3800	4.9870	4.3210	4.2320
Overshoot (OS%)	4.0300	0.8000	0.6000	0.5800
Steady-state Error	$0.42e^{-3}$	0.0013	0.0014	0.0012
Rise Time (s)	0.0650	0.1060	0.0240	0.0230

At Section A, PSO-PID settles the fastest, quickly stabilizing at the target. ZN-PID is next, while APSO-PID and FPID take a bit longer. ZN-PID overshoots the target the most, going well above it

before settling. FPID is the most accurate, with the smallest steady-state error, followed by PSO-PID. APSO-PID has a slightly larger error, and ZN-PID has the biggest. For rise time, APSO-PID is the fastest, then FPID and PSO-PID. ZN-PID is the slowest to respond. In Section B, ZN-PID and APSO-PID show small overshoots, while PSO-PID and FPID remain smooth with no overshoot. FPID again has the smallest steady-state error, closely followed by PSO-PID. ZN-PID and APSO-PID are less accurate. PSO-PID and FPID react the fastest, while ZN-PID and APSO-PID are slower. At Section C, all four controllers settle at about the same time (between 7.4 and 8.1 seconds). ZN-PID and APSO-PID show slight overshoots. PSO-PID and FPID reach the target smoothly. FPID has the smallest final error, followed by ZN-PID. PSO-PID and APSO-PID have slightly larger errors. Only ZN-PID has a measurable rise time (0.219s), showing it's the slowest to start responding. Overall, FPID is the best choice. It reacts quickly, has no overshoot, and is the most accurate. ZN-PID has decent accuracy but overshoots and reacts slowly. PSO-PID and APSO-PID settle fast but have bigger final errors than FPID.

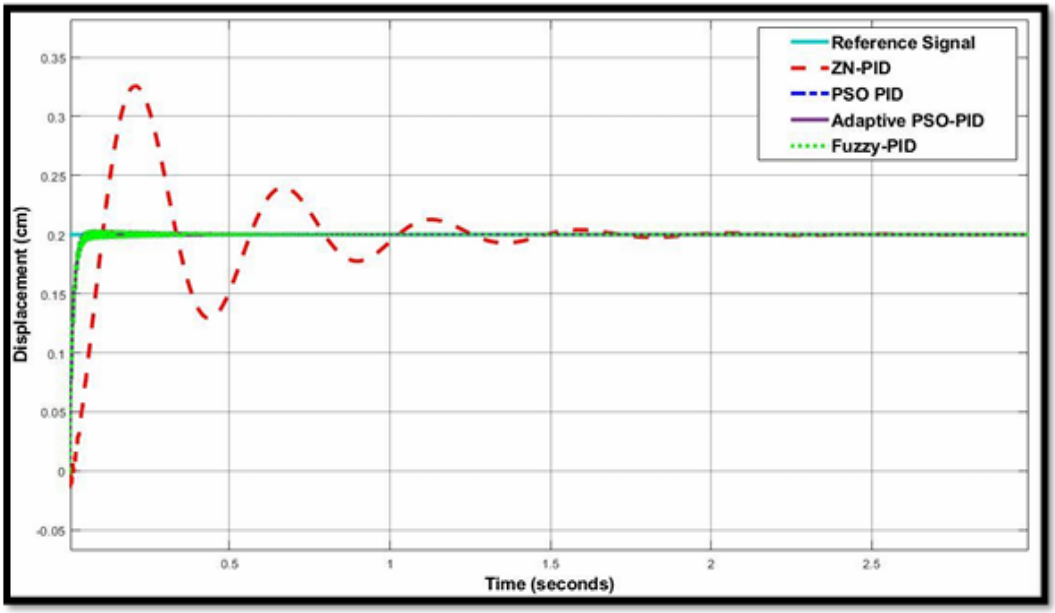

Fig. 24. The comparison between 4 methods for section A when F_L= 5000N

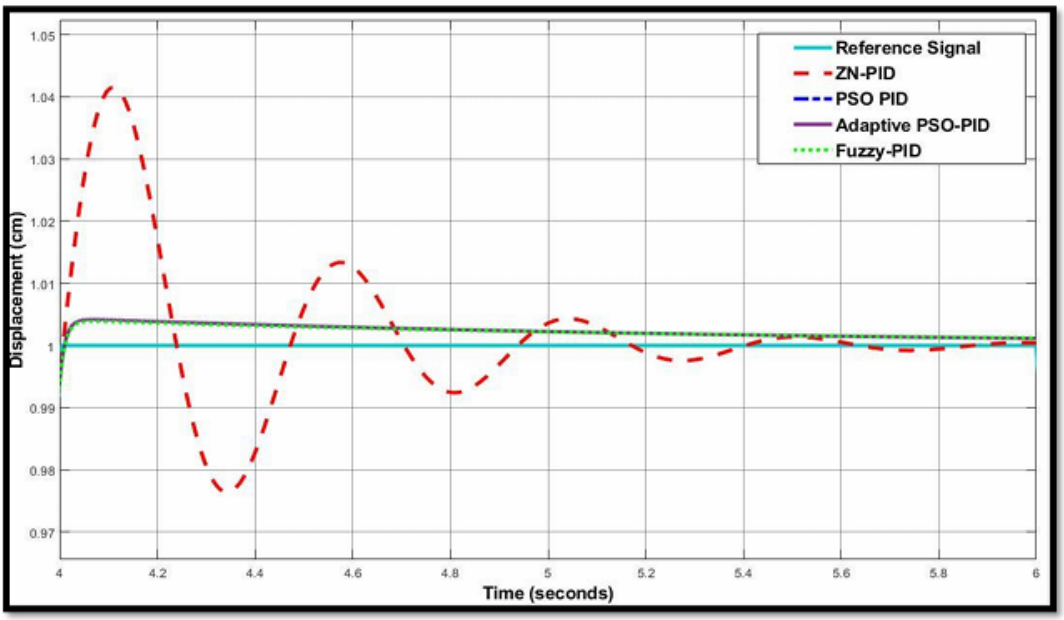

Fig. 25. The comparison between 4 methods for section B when F_L= 5000N

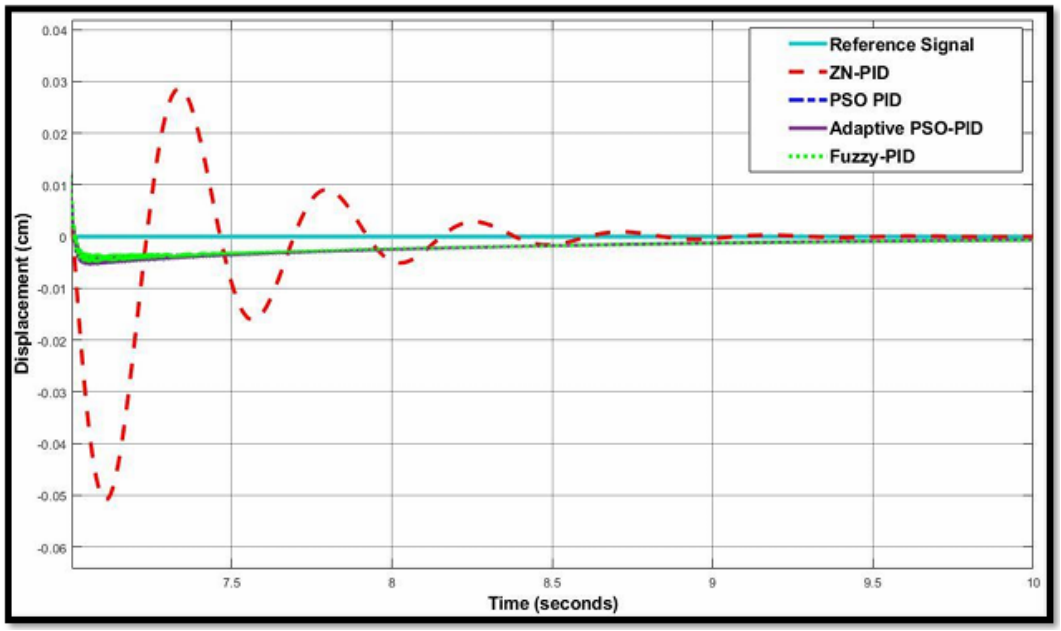

Fig. 26. The comparison between 4 methods for section C when F_L= 5000N

Table 21. Transient response analysis for step input reference signal for section C when F_L= 5000N

Gain Values	ZN-PID	PSO-PID	APSO-PID	FPID
Settling Time (s)	7.3990	8.1510	7.6300	7.5000
Overshoot (OS%)	1.0000	-	1.0400	-
Steady-state Error	$0.0026e^{-3}$	$0.6282e^{-3}$	0.0009	0.0007
Rise Time (s)	0.2190	-	-	-

3.2.4. Comparison on Transient Response When F_L = 10000N

The Fig. 27, Fig. 28, Fig. 29, Fig. 30 shows how the conventional ZN-PID, PSO-PID, APSO-PID, and FPID controllers respond when a 10000 N external disturbance is injected to the EHA system. To better highlight the differences in performance, Table 22, Table 23 and Table 24 breaks down and compares each controller's behavior in detail, dividing the transient response into three clear sections.

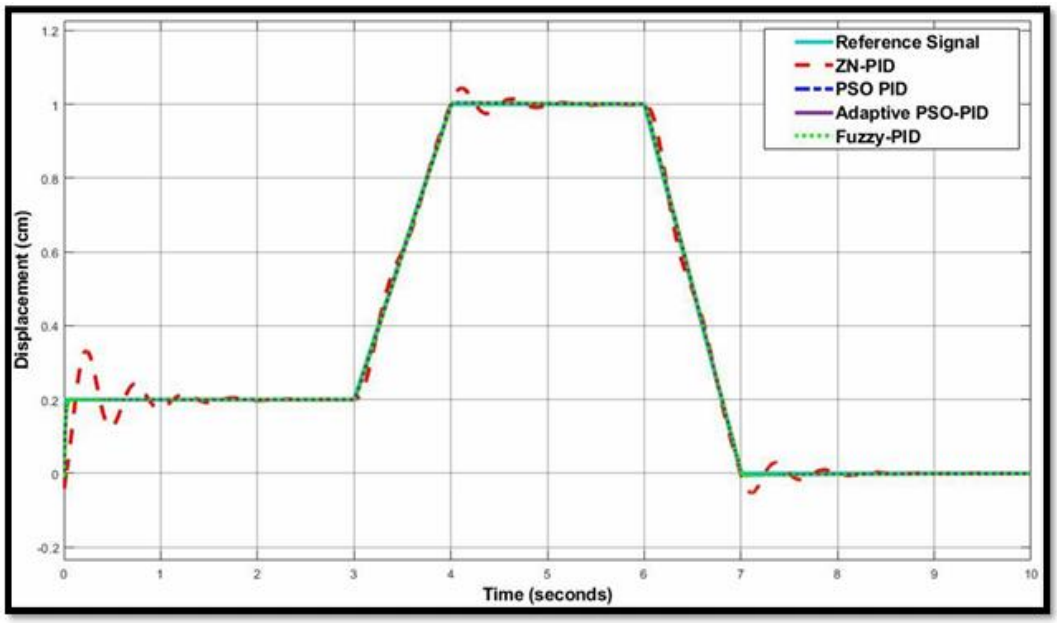

Fig. 27. The comparison between 4 methods when F_L= 10000N

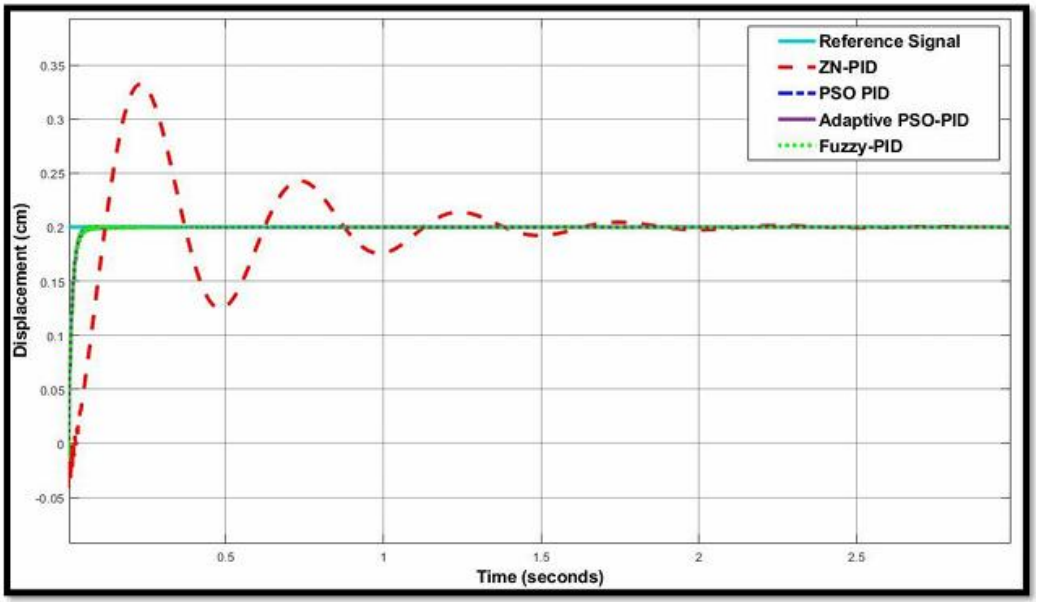

Fig. 28. The comparison between 4 methods for section A when F_L= 10000N

Table 22. Transient response analysis for step input reference signal for section A when F_L= 10000N

Gain Values	ZN-PID	PSO-PID	APSO-PID	FPID
Settling Time (s)	1.7934	0.0992	3.0000	0.0603
Overshoot (OS%)	39.9400	-	1.0400	-
Steady-state Error	$0.2480e^{-3}$	0.0030	0.0010	$0.0026e^{-3}$
Rise Time (s)	0.0761	0.0325	0.0051	0.0239

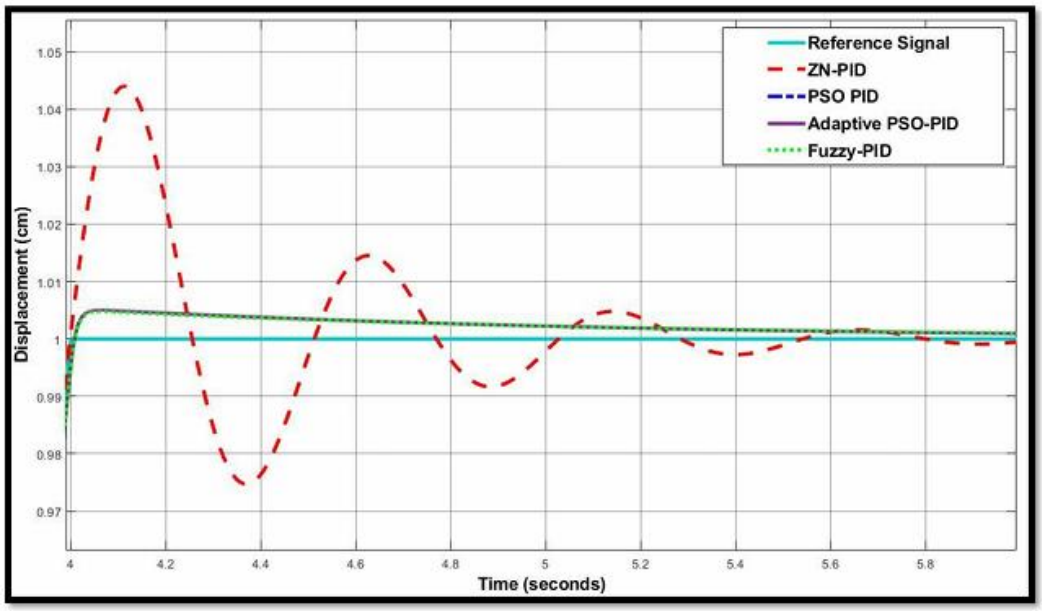

Fig. 29. The comparison between 4 methods for section B when F_L= 10000N

Table 23. Transient response analysis for step input reference signal for section B when F_L= 10000N

Gain Values	ZN-PID	PSO-PID	APSO-PID	FPID
Settling Time (s)	4.4290	4.1350	4.1270	4.1070
Overshoot (OS%)	4.2100	-	0.3900	0.0040
Steady-state Error	$0.4704e^{-3}$	0.0030	0.0014	0.0010
Rise Time (s)	0.1100	0.0270	0.0280	0.0220

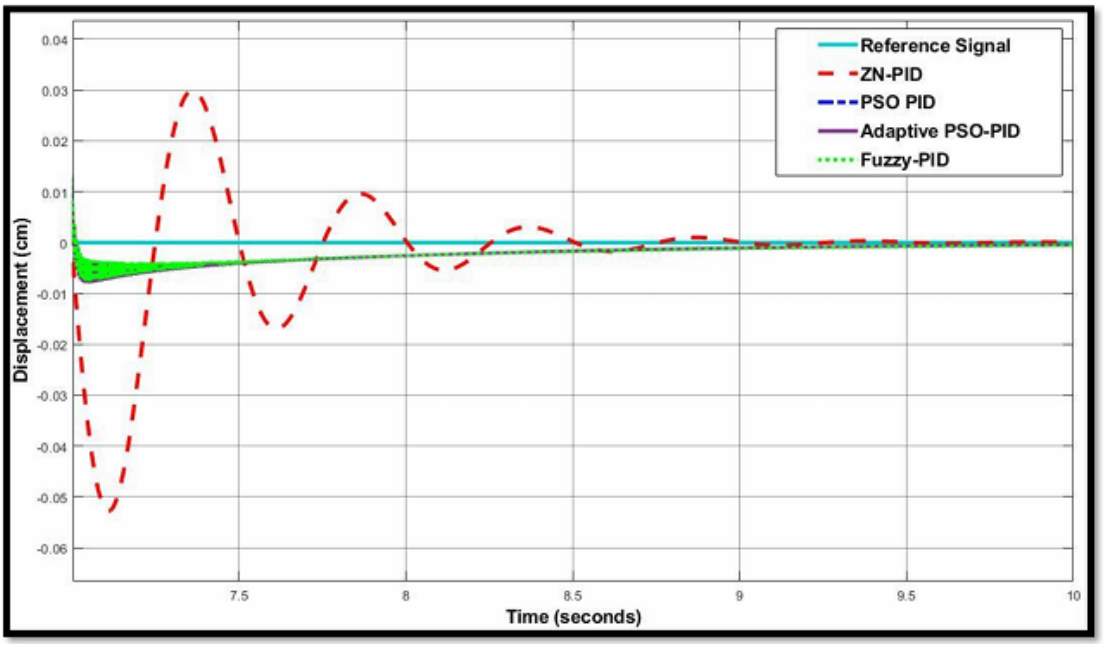

Fig. 30. The comparison between 4 methods for section C when F_L= 10000N

Table 24. Transient response analysis for step input reference signal for section C when F_L= 10000N

Gain Values	ZN-PID	PSO-PID	APSO-PID	FPID
Settling Time (s)	7.6300	7.8660	7.6540	7.3490
Overshoot (OS%)	1.0000	1.2300	1.0200	-
Steady-state Error	$0.0211e^{-3}$	0.0025	0.0008	0.0005
Rise Time (s)	0.1630	-	-	-

At Section A, PSO-PID settles the fastest, quickly stabilizing around the target. It's followed by FPID, APSO-PID, and finally ZN-PID, which takes the longest. ZN-PID also shows the biggest overshoot, going well above the target before settling. FPID is the most accurate with the smallest steady-state error, while ZN-PID has the largest. APSO-PID reacts the fastest (rise time), followed by FPID and PSO-PID. ZN-PID is the slowest to respond. In Section B, all four controllers settle at about the same speed. ZN-PID overshoots noticeably, while APSO-PID and FPID show only small overshoots. PSO-PID remains smooth with no overshoot. FPID again has the lowest steady-state error, followed by APSO-PID. PSO-PID and ZN-PID have higher errors. PSO-PID and FPID react the fastest, while ZN-PID and APSO-PID are slower. At Section C, all controllers have similar settling times. ZN-PID, PSO-PID, and APSO-PID show small overshoots, while FPID again stays smooth. FPID has the smallest steady-state error, meaning it stays closest to the target. The others have slightly larger errors, with ZN-PID being the least accurate. Only ZN-PID has a measurable rise time (0.163s), showing it's the slowest to respond. Overall, FPID is the best overall as it has no overshoot, excellent accuracy, and decent speed. PSO-PID also performs well, with a fast rise time and no overshoot, but its accuracy isn't as good. ZN-PID struggles the most due to its overshoot and higher steady-state error.

3.3. Graphical Comparisons of Varying External Disturbance Simulation

The result of custom external disturbance signal simulation used to further check the adaptability of the APSO and FPID controller based on the gain value of the K_P, K_I, and K_D is shown in Fig. 31 and Fig. 32.

3.4. Numerical Comparisons Between 4 Cases of F_L

To further analysis the performance of both controllers, the SSE value obtained from the MATLAB is compared as shown in Table 25. Based on the SSE analysis above, across all levels of

external disturbance, the FPID controller results in lower SSE values compared to the ZN-PID, PSO-PID and APSO-PID controller. It can be observed that the SSE values fluctuate more noticeably with changes in external disturbance. While the SSE values for FPID also vary with disturbance, the changes are less pronounced compared to other tested controllers. As shown in Fig. 33, the chart compares the percent improvement of PSO-PID, APSO-PID, and FPID over ZN-PID under varying external disturbances. Across all disturbance levels, FPID consistently shows the highest improvement, followed closely by APSO-PID and then PSO-PID. All three methods achieve their best performance with no disturbance (around 71–72% improvement) and experience a noticeable drop at 1000 N (around 39-41%). Performance improves again at 5000 N (approximately 62–64%) and slightly declines at 10000 N (around 50–52%). Overall, all advanced controllers significantly outperform ZN-PID, with FPID proving to be the most robust and effective across all condition.

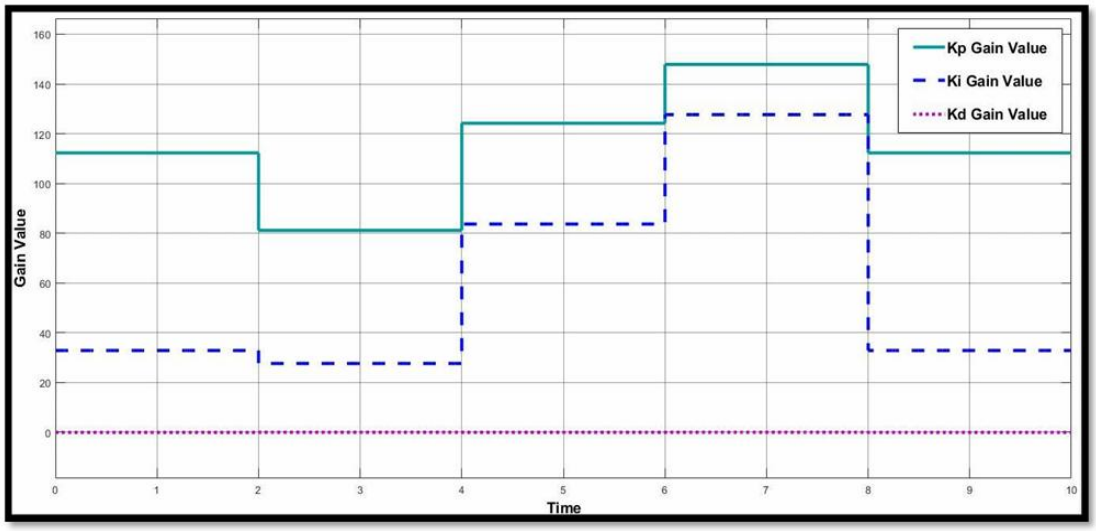

Fig. 31. The gain values for varying external disturbance with APSO-PID controller

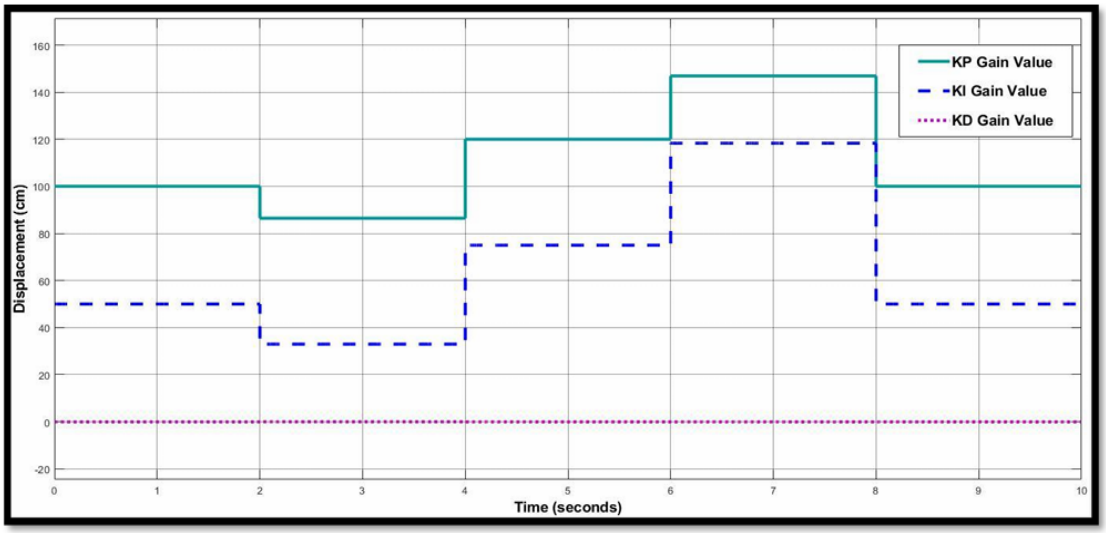

Fig. 32. The gain values for varying external disturbance with FPID controller

Table 25. SSE analysis for step input reference signal for external disturbance under 4 cases

External Disturbance,F_L	ZN-PID	PSO-PID	APSO-PID	FPID
0 N	4.3079	1.2479	1.2301	1.1985
1000 N	1.9749	1.1961	1.1868	1.1694
5000 N	3.2644	1.2431	1.2107	1.1875
10000 N	2.8256	1.4219	1.3764	1.3481

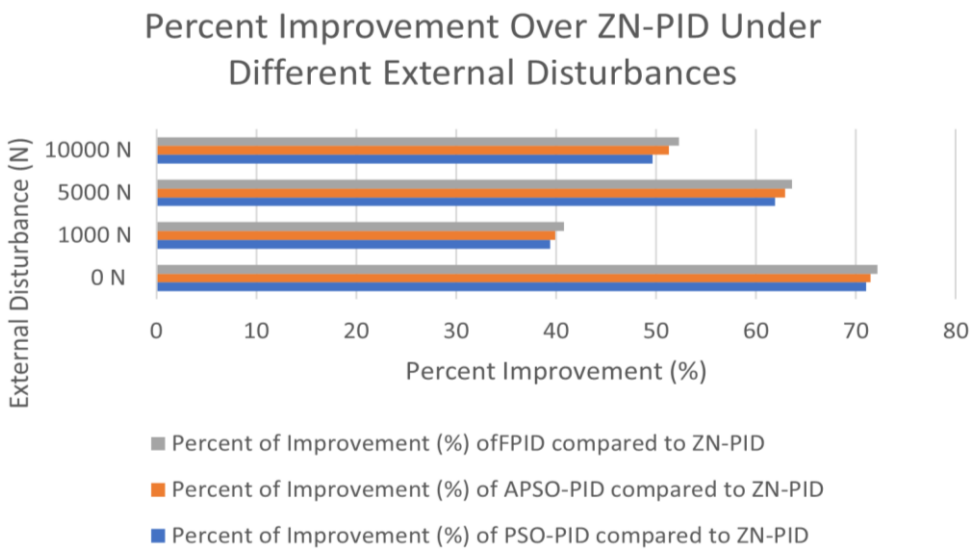

Fig. 33. The percentage improvement of PSO-PID, APSO-PID, and FPID under various external disturbances

3.5. Summary

The performance of the ZN-PID, PSO-PID, APSO-PID, and FPID controllers was evaluated under external disturbances of 0 N, 1000 N, 5000 N, and 10000 N using transient response analysis. Across all disturbance levels, the FPID controller consistently exhibited superior performance, characterized by faster settling time, negligible overshoot, and the lowest steady-state error. The PSO-PID controller demonstrated competitive transient behaviour, particularly in rise time and settling characteristics, but showed comparatively higher steady-state errors in some cases. Although the APSO-PID controller achieved very fast rise times and strong performance under specific operating conditions, its response was less consistent across increasing disturbance levels. The ZN-PID controller consistently yielded inferior performance due to pronounced overshoot, slower dynamics, and higher steady-state error. In this study, robustness is defined as the ability of the controller to maintain low tracking error and stable transient behaviour as disturbance magnitude increases. Accordingly, robustness is evaluated using time-domain and error-based indices, specifically variations in steady-state error, sum of squared error (SSE), and transient response characteristics under escalating external loads. Frequency-domain robustness margins, such as gain and phase margins, are not considered in this work and are identified as a potential direction for future research. While APSO-PID exhibits superior performance in isolated cases, overall robustness is assessed based on consistency across all disturbance scenarios rather than peak performance. From this perspective, the FPID controller demonstrates the most stable and repeatable behaviour. The stochastic optimization processes used for PSO-PID and APSO-PID tuning exhibited consistent convergence behaviour within the selected iteration limits, indicating reliable parameter optimization. While stochastic variability is inherent in PSO-based methods, the reported results were repeatable across multiple optimization trials with consistent ranking trends. The comparative results further confirm that intelligent PID tuning strategies outperform conventional Ziegler–Nichols tuning for electro-hydraulic actuator systems operating under variable load conditions. Overall, the FPID controller emerges as the most robust and effective control strategy among the evaluated methods, offering a balanced trade-off between fast transient response, minimal overshoot, and high tracking accuracy under increasing external disturbances.

4. Conclusion

This study investigated multiple control strategies for an Electro-Hydrostatic Actuator (EHA) system subjected to disturbance forces ranging from 0 N to 10,000 N using a MATLAB/Simulink model. A conventional Ziegler–Nichols PID controller provided basic stability but exhibited

degraded performance under high disturbances. The PSO-PID and APSO-PID controllers improved transient response and robustness, with APSO-PID benefiting from disturbance-dependent parameter adaptation. Among all methods, the Fuzzy-PID (FPID) controller demonstrated the best overall performance, achieving the fastest settling time, minimal overshoot, and the highest tracking accuracy. The primary theoretical contribution of this work is a systematic comparison of classical, optimisation-based, and intelligence-based PID control strategies for disturbance-intensive EHA systems, highlighting the effectiveness of fuzzy logic–based adaptive tuning in addressing external disturbances. The superior disturbance rejection capability of the FPID controller underscores its potential for high-precision applications such as aerospace actuation, robotics, and advanced industrial systems. Despite these promising results, the study is limited to simulation-based evaluation and a restricted set of performance metrics. Practical implementation of FPID controllers may be influenced by sensor noise, computational latency, nonlinear leakage, and uncertainties in fuzzy rule design. Future research should therefore focus on experimental validation using real or hardware-in-the-loop EHA systems, the inclusion of additional metrics such as energy efficiency and robustness, the exploration of alternative intelligent optimization techniques, and the integration of fault detection and diagnosis mechanisms to enhance reliability and real-world applicability.

Author Contribution: All authors contributed equally to the main contributor to this paper. All authors read and approved the final paper.

Data Availability: The data used to support the findings of this study are available at reasonable request from the corresponding author.

Conflicts of Interest: The authors declare that they have no conflicts of interest.

Funding: The authors gratefully acknowledge the support and research facilities provided by Universiti Malaysia Perlis (UNIMAP) and Universiti Teknologi Malaysia (UTM).

References

[1] H. Razmjooei, G. Palli, and M. Nazari, "Disturbance observer-based mismatched feedback control for position tracking of electro-hydraulic systems in a finite time," *European Journal of Control*, vol. 67, p. 100659, 2022, https://doi.org/10.1016/j.ejcon.2022.100659.

[2] Z. Yao, X. Liang, Q. Zhao, and J. Yao, "Adaptive disturbance observer-based control of hydraulic systems with asymptotic stability," *Applied Mathematical Modelling*, vol. 105, pp. 226-242, 2022, https://doi.org/10.1016/j.apm.2021.12.026.

[3] Z. Xu, G. Qi, Q. Liu, and J. Yao, "Output feedback disturbance rejection control for full-state constrained hydraulic systems with guaranteed tracking performance," *Applied Mathematical Modelling*, vol. 111, pp. 332-348, 2022, https://doi.org/10.1016/j.apm.2022.06.043.

[4] G. Palli, S. Strano, and M. Terzo, "A novel adaptive-gain technique for high-order sliding-mode observers with application to electro-hydraulic systems," *Mechanical Systems and Signal Processing*, vol. 144, p. 106875, 2020, https://doi.org/10.1016/j.ymssp.2020.106875.

[5] S. Qu, D. Fassbender, A. Vacca, and E. Busquets, "A Cost-Effective Electro-Hydraulic Actuator Solution with Open Circuit Architecture," *International Journal of Fluid Power*, vol. 22, no. 2, pp. 233-258, 2021, https://doi.org/10.13052/ijfp1439-9776.2224.

[6] L. Li *et al*., "Research on Electro-Hydraulic Ratios for A Novel Mechanical-Electro-Hydraulic Power Coupling Electric Vehicle," *Energy*, vol. 270, p. 126970, 2023, https://doi.org/10.1016/j.energy.2023.126970.

[7] K. Abuowda, I. Okhotnikov, S. Noroozi, P. Godfrey, and M. Dupac, "A review of electrohydraulic independent metering technology," *ISA Transactions*, vol. 98, pp. 364-381, 2020, https://doi.org/10.1016/j.isatra.2019.08.057.

[8] M. H. Nguyen and K. K. Ahn, "Output Feedback Robust Tracking Control for a Variable-Speed Pump-Controlled Hydraulic System Subject to Mismatched Uncertainties," *Mathematics*, vol. 11, no. 8, p. 1783, 2023, https://doi.org/10.3390/math11081783.

[9] E. O. Ogunniyi and B. S. Richards, "Renewable energy powered membrane technology: Electro-hydraulic control system design for managing pump shutdowns in a photovoltaic-membrane water desalination system," *Desalination*, vol. 608, p. 118784, 2025, https://doi.org/10.1016/j.desal.2025.118784.

[10] T. Yin, X. Zhang, and D. Huang, "Load-sensitive impedance control for resilient force balance in variable displacement electrohydrostatic actuators," *Control Engineering Practice*, vol. 162, p. 106329, 2025, https://doi.org/10.1016/j.conengprac.2025.106329.

[11] H. Xiong, H. Zheng, D. Zhao, and Y. Feng, "Optimized Control Strategy for Electro-hydraulic Servo Active Suspension System With Internal Leakage Faults," *International Journal of Control, Automation, and Systems*, vol. 23, pp. 1893-1907, 2025, https://doi.org/10.1007/s12555-024-0821-4.

[12] M. H. Nguyen and K. K. Ahn, "A Novel Trajectory Adjustment Mechanism-Based Prescribed Performance Tracking Control for Electro-Hydraulic Systems Subject to Disturbances and Modeling Uncertainties," *Applied Sciences*, vol. 12, no. 12, p. 6034, 2022, https://doi.org/10.3390/app12126034.

[13] K. Zhang, J. Zhang, M. Gan, H. Zong, X. Wang, H. Huang, Q. Su, and B. Xu, "Modeling and Parameter Sensitivity Analysis of Valve-Controlled Helical Hydraulic Rotary Actuator System," *Chinese Journal of Mechanical Engineering*, vol. 35, no. 66, 2022, https://doi.org/10.1186/s10033-022-00737-w.

[14] S. W. Shneen, H. H. Juhi, and H. A. Najim, "Simulation and Modeling with Designing for the Proportional, Integral and Derivative Control of Industrial Robotic Arm by Using MATLAB/Simulink," *International Journal of Robotics and Control Systems*, vol. 4, no. 4, pp. 2073-2094, 2024, https://doi.org/10.1186/s10033-022-00737-w.

[15] Y. Yang, K. Cui, D. Shi, G. Mustafa, and J. Wang, "PID control with PID event triggers: Theoretic analysis and experimental results," *Control Engineering Practice*, vol. 128, p. 105322, 2022, https://doi.org/10.1016/j.conengprac.2022.105322.

[16] A. K. Kumawat, R. Kumawat, M. Rawat, and R. Rout, "Real time position control of electrohydraulic system using PID controller," *Materials Today: Proceedings*, vol. 47, pp. 2966-2969, 2021, https://doi.org/10.1016/j.matpr.2021.05.203.

[17] W. Ma, S. Ma, W. Qiao, D. Cao, and C. Yin, "Research on PID Controller of Excavator Electro-Hydraulic System Based on Improved Differential Evolution," *Machines*, vol. 11, no. 2, p. 143, 2023, https://doi.org/10.3390/machines11020143.

[18] J. Li, W. Li, H. Liang, and L. Kong, "Review of Research on Improved PID Control in Electro-hydraulic Servo System," *Recent Patents on Engineering*, vol. 18, no. 1, pp. 54-68, 2024, http://dx.doi.org/10.2174/1872212117666230210090351.

[19] H. Feng, W. Ma, C. Yin, and D. Cao, "Trajectory control of electro-hydraulic position servo system using improved PSO-PID controller," *Automation in Construction*, vol. 127, p. 103722, 2021, https://doi.org/10.1016/j.autcon.2021.103722.

[20] E. S. Rahayu, A. Ma'arif, and A. Cakan, "Particle Swarm Optimization (PSO) Tuning of PID Control on DC Motor," *International Journal of Robotics and Control Systems*, vol. 2, no. 2, pp. 435-447, 2022, https://doi.org/10.31763/ijrcs.v2i2.476.

[21] P. Chotikunnan *et al*., "Enhancing MG996R Servo Motor Performance Using PSO-Tuned PID and Feedforward Control," *International Journal of Robotics and Control Systems*, vol. 5, no. 2, pp. 1120-1138, 2025, https://doi.org/10.31763/ijrcs.v5i2.1854.

[22] U. Kruthika and S. Paneerselvam, "Improved Adaptive PSO-based Gain Tuning for PID Controllers in Utility Boilers," *Procedia Computer Science*, vol. 203, pp. 183-192, 2023, https://doi.org/10.1016/j.procs.2023.12.073.

[23] R. Liu, L. Wei, and P. Zhang, "An adaptive particle swarm optimization with information interaction mechanism," *Machine Learning: Science and Technology*, vol. 5, no. 2, pp. 1-26, 2024, https://doi.org/10.1088/2632-2153/ad55a5.

[24] M. S. Amiri, R. Ramli, M. Ibrahim, D. A. Wahab, and N. Aliman, "Adaptive Particle Swarm Optimization of PID Gain Tuning for Lower-Limb Human Exoskeleton in Virtual Environment," *Mathematics*, vol. 8, no. 11, p. 2040, 2020, https://doi.org/10.3390/math8112040.

[25] K. Ye and P. Li, "A new adaptive PSO-PID control strategy of hybrid energy storage system for electric vehicles," *Advances in Mechanical Engineering*, vol. 12, no. 9, pp. 1-15, 2020, https://doi.org/10.1177/1687814020958574.

[26] N. H. M. Ali *et al*., "Enhanced Hybrid Robust Fuzzy-PID Controller for Precise Trajectory Tracking Electro-Hydraulic Actuator System," *International Journal of Robotics and Control Systems*, vol. 4, no. 2, pp. 795-813, 2024, https://doi.org/10.31763/ijrcs.v4i2.1407.

[27] A. Irawan, M. S. Ramli, M. H. Sulaiman, M. I. P. Azahar, A. H. Adom, "Optimal Pneumatic Actuator Positioning and Dynamic Stability using Prescribed Performance Control with Particle Swarm Optimization: A Simulation Study," *International Journal of Robotics and Control Systems*, vol. 3, no. 3, pp. 364-379, 2023, https://doi.org/10.31763/ijrcs.v3i3.1002.

[28] H. Zhang, L. Ding, W. Zhang, and C. Li, "Performance analysis of an electro-hydrostatic actor with high-pressure load sensing based on fuzzy PID," *Mechanical Sciences*, vol. 12, no. 1, pp. 529-537, 2021, https://doi.org/10.5194/ms-12-529-2021.

[29] T. N. Van, H. Q. Tran, V. X. Ha, C. Ha, P. H. Minh, "Fuzzy Feedback Control for Electro-Hydraulic Actuators," *Intelligent Automation & Soft Computing*, vol. 36, no. 2, pp. 2441-2456, 2023, https://doi.org/10.32604/iasc.2023.033368.

[30] M. Elouni, H. Hamdi, B. Rabaoui, and N. B. Braiek, "Adaptive PID Fault-Tolerant Tracking Controller for Takagi-Sugeno Fuzzy Systems with Actuator Faults: Application to Single-Link Flexible Joint Robot," *International Journal of Robotics and Control Systems*, vol. 2, no. 3, pp. 523-546, 2022, https://doi.org/10.31763/ijrcs.v2i3.762.

[31] N. H. M. Ali, H. I. Jaafar, R. Ghazali, M. F. Ghani, C. C. Soon, Z. Has, "Identification and Control of Industrial Hydraulic Actuators with a Hammerstein-Wiener Model Approach," *Systems Modelling and Simulation*, vol. 2483, pp. 131-145, 2024, https://doi.org/10.1007/978-981-96-4613-5_10.

[32] Z. Wu, B. Jiao, C. Sun, Y. Zhang, and H. Zhao, "Design and Optimization of Hydropneumatic Suspension Simulation Test Bench with Electro-Hydraulic Proportional Control," *Machines*, vol. 11, no. 9, p. 907, 2023, https://doi.org/10.3390/machines11090907.

[33] S. Jiang, H. Shen, S. Zhi, C. Cheng, H. Ren, J. Tong, "Research on Compliance Control of Electro-Hydraulic Loading Experimental System," *Electronics*, vol. 13, no. 7, p. 1273, 2024, https://doi.org/10.3390/electronics13071273.

[34] J. Li, L. Kong, H. Liang, and W. Li, "Review of Development and Characteristics Research on Electro-hydraulic Servo System," *Recent Patents on Engineering*, vol. 18, no. 6, pp. 140-154, 2024, http://dx.doi.org/10.2174/1872212118666230711165517.

[35] Z. Xu, G. Qi, Q. Liu, and J. Yao, "Output feedback disturbance rejection control for full-state constrained hydraulic systems with guaranteed tracking performance," *Applied Mathematical Modelling*, vol. 111, pp. 332-348, 2022, https://doi.org/10.1016/j.apm.2022.06.043.

[36] M. H. Nguyen, H. V. Dao, and K. K. Ahn, "Active Disturbance Rejection Control for Position Tracking of Electro-Hydraulic Servo Systems under Modeling Uncertainty and External Load," *Actuators*, vol. 10, no. 2, p. 20, 2021, https://doi.org/10.3390/act10020020.

[37] N. H. M. Ali, R. Ghazali, H. I. Jaafar, M. F. Ghani, C. C. Soon, Z. Has, "Comparison Study between Open-Loop and Closed-Loop Identification for Industrial Hydraulics Actuator System," *International Journal of Mechanical Engineering and Robotics Research*, vol. 13, no. 5, pp. 516-521, 2024, https://doi.org/10.18178/ijmerr.13.5.516-521.

[38] H. Khan, S. J. Abbasi, and M. C. Lee, "Control of an Assistive Robot for Paraplegics Using PID Controller with Sliding Perturbation Observer," *International Journal of Mechanical Engineering and Robotics Research*, vol. 10, no. 4, pp. 196-201, 2021, https://doi.org/10.18178/ijmerr.10.4.196-201.

[39] P. Bury, M. Stosiak, K. Urbanowicz, A. Kodura, M. Kubrak, and A. Malesińska, "A case study of open- and closed-loop control of hydrostatic transmission with proportional valve start-up process," *Energies*, vol. 15, no. 1, p. 1860, 2022, https://doi.org/10.3390/en15051860.

[40] J. Liu, J. Yao, and W. Deng, "Nonlinear Robust Adaptive Control of Electro-hydrostatic Actuators With Continuous Friction Compensation," *International Journal of Control, Automation, and Systems*, vol. 22, pp. 1225-1237, 2024, https://doi.org/10.1007/s12555-022-1120-6.

[41] V. D. Phan and K. K. Ahn, "Optimized-Based Fault-Tolerant Control of an Electro-Hydraulic System with Disturbance Rejection," *Applied Sciences*, vol. 12, no. 18, p. 9197, 2022, https://doi.org/10.3390/app12189197.

[42] E. W. Suseno and A. Ma'arif, "Tuning of PID Controller Parameters with Genetic Algorithm Method on DC Motor," *International Journal of Robotics and Control Systems*, vol. 1, no. 1, pp. 41-53, 2021, https://doi.org/10.31763/ijrcs.v1i1.249.

[43] W. Wu, G. Gong, Q. Huan, X. Zhou, Y. Chen, and X. Peng, "Investigation into the electrohydraulic synchronous motion control of a thrust system for a tunnel boring machine," *Machines*, vol. 10, no. 2, p. 119, 2022, https://doi.org/10.3390/machines10020119.

[44] M. H. Setiawan, A. Ma'arif, M. F. Saifuddin, and W. A. Salah, "A Comparative Study of PID, FOPID, ISF, SMC, and FLC Controllers for DC Motor Speed Control with Particle Swarm Optimization," *International Journal of Robotics and Control Systems*, vol. 5, no. 1, pp. 640-660, 2025, https://doi.org/10.31763/ijrcs.v5i1.1764.

[45] X. B. Zou, S. D. Mohanty, H. G. Luo, and Y. X. Liu, "Swarm intelligence methods for extreme mass ratio inspiral search: first application of particle swarm optimization," *Universe*, vol. 10, no. 2, p. 96, 2024, https://doi.org/10.3390/universe10020096.

[46] H. R. Kaviani and M. Moshfeghi, "Multi-Megawatt Horizontal Axis Wind Turbine Blade Optimization Based on PSO Method," *Aerospace*, vol. 10, no. 2, p. 158, 2023, https://doi.org/10.3390/aerospace10020158.

[47] G. Rossides, B. Metcalfe, and A. Hunter, "Particle Swarm Optimization-An Adaptation for the Control of Robotic Swarms," *Robotics*, vol. 10, no. 2, p. 58, 2021, https://doi.org/10.3390/robotics10020058.

[48] A. Okhitina, D. Roldugin, and S. Tkachev, "Application of the PSO for the construction of a 3-axis stable magnetically actuated satellite angular motion," *Acta Astronautica*, vol. 195, pp. 86-97, 2022, https://doi.org/10.1016/j.actaastro.2022.03.001.

[49] M. EL-Qasery, A. Abbou, M. Laamim, L. Id-Khajine, and A. Rochd, "Comparative analysis of GA and PSO algorithms for optimal cost management in on-grid microgrid energy systems with PV-battery integration," *Global Energy Interconnection*, vol. 8, no. 4, pp. 572-580, 2025, https://doi.org/10.1016/j.gloei.2025.05.003.

[50] Z. Jiang, D. Zhu, X.-Y. Li, and L.-B. Han, "A Hybrid Adaptive Particle Swarm Optimization Algorithm for Enhanced Performance," *Applied Sciences*, vol. 15, no. 11, p. 6030, 2025, https://doi.org/10.3390/app15116030.

[51] B. Cai, X. Zhu, and Y. Qin, "Parameters optimization of hybrid strategy recommendation based on particle swarm algorithm," *Expert Systems with Applications*, vol. 168, p. 114388, 2021, https://doi.org/10.1016/j.eswa.2020.114388.

[52] M. Z. Fadel, "Hybrid Control Algorithm Sliding Mode-PID for an Electrohydraulic Servo Actuator System Based on Particle Swarm Optimization Technique," *Journal Européen des Systèmes Automatisés*, vol. 56, no. 1, pp. 153-163, 2023, https://doi.org/10.18280/jesa.560119.

[53] J. Miao, J. Wang, D. Wang, and Q. Miao, "Experimental investigation on electro-hydraulic actuator fault diagnosis with multi-channel residuals," *Measurement*, vol. 180, p. 109544, 2021, https://doi.org/10.1016/j.measurement.2021.109544.

[54] V. D. Phan, C. P. Vo, H. V. Dao and K. K. Ahn, "Robust Fault-Tolerant Control of an Electro-Hydraulic Actuator With a Novel Nonlinear Unknown Input Observer," *IEEE Access*, vol. 9, pp. 30750-30760, 2021, https://doi.org/10.1109/ACCESS.2021.3059947.

[55] Y. Song, Z. Hu, and C. Ai, "Fuzzy Compensation and Load Disturbance Adaptive Control Strategy for Electro-Hydraulic Servo Pump Control System," *Electronics*, vol. 11, no. 7, p. 1159, 2022, https://doi.org/10.3390/electronics11071159.

[56] J. Tavoosi *et al*., "A New General Type-2 Fuzzy Predictive Scheme for PID Tuning," *Applied Sciences*, vol. 11, no. 21, p. 10392, 2021, https://doi.org/10.3390/app112110392.

[57] E. Chavero-Navarrete, M. Trejo-Perea, J. C. Jáuregui-Correa, R. V. Carrillo-Serrano, G. Ronquillo-Lomeli, and J. G. Ríos-Moreno, "Hierarchical pitch control for small wind turbines based on fuzzy logic and anticipated wind speed measurement," *Applied Sciences*, vol. 10, no. 13, p. 4592, 2020, https://doi.org/10.3390/app10134592.

[58] H. D. Choi and S. H. You, "Fuzzy Finite Memory State Estimation for Electro-Hydraulic Active Suspension Systems," *IEEE Access*, vol. 9, pp. 99364-99373, 2021, https://doi.org/10.1109/ACCESS.2021.3096184.

[59] S. Liu, R. Hao, D. Zhao and Z. Tian, "Adaptive Dynamic Surface Control for Active Suspension With Electro-Hydraulic Actuator Parameter Uncertainty and External Disturbance," *IEEE Access*, vol. 8, pp. 156645-156653, 2020, https://doi.org/10.1109/ACCESS.2020.3018442.

[60] V. K. Nguyen, V. K. Tran, H. Pham, H. D. Nguyen, and C. N. Nguyen, "Design and Implementation of Fuzzy-based Fine-tuning PID Controller for Programmable Logic Controller," *International Journal of Integrated Engineering*, vol. 16, no. 5, pp. 359-372, 2024, https://doi.org/10.30880/ijie.2024.16.05.027.